DEVELOPMENT OF A COMPACT TIME-DOMAIN TERAHERTZ SPETROMETER USING PHOTOCONDUCTIVE ANTENNA DETECTION METHOD

A THESIS SUBMITTED TO
THE GRADUATE SCHOOL OF NATURAL AND APPLIED SCIENCES
OF
MIDDLE EAST TECHNICAL UNIVERSITY

BY

ÜMMÜGÜL ERÖZBEK-GÜNGÖR

IN PARTIAL FULFILLMENT OF THE REQUIREMENTS
FOR
THE DEGREE OF MASTER OF SCIENCE
IN
PHYSICS

February 2009

Approval of the Thesis

submitted by **ÜMMÜGÜL ERÖZBEK GÜNGÖR** in partial fulfillment of the requirements for the degree of **Master of Science in Physics Department, Middle East Technical University** by,

Prof. Dr. Canan Özgen _____
Dean, Graduate School of **Natural and Applied Sciences**

Prof. Dr. Sinan Bilikmen _____
Head of Department, **Physics**

Dr. Hakan Altan _____
Supervisor, **Physics Dep., METU**

Prof. Dr. Sinan Bilikmen _____
Co-Supervisor, **Physics Dep., METU**

Examining Committee Members:

Prof. Dr. Sinan Bilikmen _____
Physics Dept., METU

Dr. Hakan Altan _____
Physics Dept., METU

Assoc. Prof. Özlem Aydın Çivi _____
Elec. Electr. Engineering Dept., METU

Dr. Halil Berberoğlu _____
Physics Dept. METU

Dr. Demiral Akbar _____
Physics Dept. METU

Date: 13 February 2009

I hereby declare that all information in this document has been obtained and presented in accordance with academic rules and ethical conduct. I also declare that, as required by these rules and conduct, I have fully cited and referenced all material and results that are not original to this work.

Name, Last Name: Ümmügül ERÖZBEK GÜNGÖR

Signature :

ABSTRACT

DEVELOPMENT OF A COMPACT TIME-DOMAIN TERAHERTZ SPECTROMETER USING PHOTOCONDUCTIVE ANTENNA DETECTION METHOD

Güngör Erözbek, Ümmügül
M. S. Department of Physics
Supervisor: Dr. Hakan ALTAN
Co-Supervisor: Prof. Dr. Sinan BİLİKMEN

February 2009, 54 pages

In this thesis, we describe the development of a time-domain terahertz (THz) spectrometer driven by two different laser sources: an Er-doped femtosecond fiber laser and a mode-locked Ti:Sapphire laser. The resulting THz electromagnetic radiation was generated and detected using photoconductive antenna detection methods in both systems. In these experiments we characterized the THz power output for both the fiber laser driven system and the Ti:Sapphire laser driven system. Emphasis is given throughout this thesis on understanding the working principles behind time-domain terahertz spectroscopy, applications of THz radiation and terahertz generation as well as terahertz detection methods.

We calculated the THz power output using two different methods. By using the "Hertzian Dipole" method we estimated the generated THz power after the generation photoconductive antenna. Using this method, we showed that the

generated power is on the order of milliwatts, which is far larger than the expected power typical for these systems. The second, “Open-Circuit Voltage” method, allowed us to calculate the received power on the detection photoconductive antenna. Using this method we were able to show that the THz power generated and detected in these systems is on the order of microwatts. For the mode-locked fiber laser driven spectrometer we obtained on average a ~ 4 ps (0.25 THz) pulse length which corresponded to an average power in the range of 71.8 nW - 70.54 μW on a dipole antenna with a 6 μm dipole gap and 44 μm dipole length. Using the mode-locked Ti:Sapphire laser driven spectrometer we observed a ~ 2 ps (0.5 THz) pulse length and average power in the range of 0.54 nW – 5.12 μW on a different dipole antenna with a 5 μm gap and 40 μm dipole length. Since these values agree with expected values for these systems we believe the “Open-Circuit Voltage” method is appropriate when trying to calculate the THz power.

Keywords: THz, THz-TDS, photoconductive antenna detection method, power characterization.

ÖZ

FOTOİLETKEN ANTEN BELİRLEME YÖNTEMİ İLE KOMPAKT ATILIMLI TERAHERTZ SPEKTROMETRE GELİŞTİRME PROJESİ

Güngör Erözbek, Ümmügül
Yüksek Lisans, Fizik Bölümü
Tez Yöneticisi: Dr. Hakan ALTAN
Ortak Tez Yöneticisi: Prof. Dr. Sinan BİLİKMEN

Şubat 2009, 54 sayfa

Biz bu tezde iki farklı lazer kaynağı (Erbiyum katkılı kip kilitli fiber lazer ve Titanyum Safir mod kilitli lazer) kullanarak kompakt atılımlı terahertz spektrometre geliştirilmeye çalıştik. Her iki sistemde de THz dalga boylarını elde etmek ve belirlemek için fotoiletken belirleme yöntemi kullandık. Bu deneylerde, her iki lazer kullanarak elde edilen THz güç çıkışlarını karakterize ettik. Bu tez boyunca, kopakt atılımlı terahertz spektrometresinin arkasındaki çalışma prensiplerine, terahertz uygulamalarına, terahertz üretim ve terahertz belirleme metotlarına yoğunlaşıldı.

İki farklı yöntem kullanarak THz güç çıkışlarını hesapladık. "Hertz dipol" metotunu kullanarak, üretici fotoiletken antenden yayılan THz radyasyonunun gücünü tahmin ettik. Bu metotla, üretilen gücün bu deneyler için beklenen tipik güç değerlerinden çok uzak olan milivat mertebesinde olduğunu gösterdik. İkinci (Açık devre gerilim) metotla belirleyici fotoiletken antenden yayılan gücü hesapladık. Bu metotla, bu sistemlerde üretilen ve belirlenen THz

radyasyonunun gücünün mikrovat mertebesinde olduğunu gösterebildik. Mod kilitli fiber lazerle gerçekleştirilen spektrometre için, ortalama yaklaşık 4 ps genişliğinde 0.25 THz ve dipol aralığı 6 μm, dipol uzunluğu 44 μm olan dipol anten üzerinde ortalama gücü 71.8 nW - 70.54 μW aralığında olan THz dalga boyları elde ettik. Mod kilitli Titanyum Safir lazer kullanarak gerçekleştirilen spektrometre için, yaklaşık 2 ps genişliğinde 0.5 THz ve dipol aralığı 5 μm, dipol uzunluğu 40 μm olan farklı dipol anten üzerinde ortalama gücü 0.54 nW – 5.12 μW aralığında olan THz dalga boylarını gözledik. Bu değerler bu tip sistemler için beklenen değerlerle örtüştüğünden biz THz dalga boylarının gücünü hesaplarken "Açık devre gerilim" hesaplama metotunun daha uygun olduğuna inandık.

Anahtar Sözcükler: Terahertz, kompakt atılımlı terahertz spektrometre, fotoiletken anten belirleme yöntemi, güç karakterizasyonu

To my lovely family ...

ACKNOWLEDGEMENTS

I would like to express my gratitude to my supervisor, Hakan ALTAN for his patience and his support during the work and also for his great satisfactory knowledge about the concept. Also, I would like to thank TÜBİTAK for their 107T742 project support.

I would like to thank, firstly, Prof. Dr. Sinan BİLİKMEN for his guidance and support. Secondly, I thank to Dr. Demiral AKBAR and Dr. Halil BERBEROĞLU for their friendly behaviors, discussions and supports. The other person who I want to thank is my laboratory study partner, Mukaddes Meliz AKBULUT, for her productive teamwork and also I want to thank Zahide TOSUN for her confidence.

My special thanks go to the people who are very important in my life, my lovely family and especially my husband (Özgür GÜNGÖR), for their confidence, supports, pains and their endless love and patience.

Lastly, I would like to thank my neighbors Mustafa BAYRAK and Emine BAYRAK for their endless confidence, supports and their love.

TABLE OF CONTENTS

LIST OF TABLES

LIST OF FIGURES

LIST OF SYMBOLS AND ABBREVIATIONS

THz : Terahertz (10^{12} Hz)

Hz : Hertz

PCA : Photoconductive Antenna

T-ray : Terahertz Radiation

DNA : Deoxyribonucleic Acid

NASA : National Aeronautics and Space Administration

TSA : Transportation Security Administration

X-ray : X radiation

THz-TDS : Terahertz Time Domain Spectroscopy

SNR : Signal to Noise Ratio

Ti : Titanium

IR : Infrared

OR : Optical Rectification

$LiNbO_3$: Lithium Niobate

$LiTaO_3$: Lithium Tantalate

GaAs : Gallium Arsenide

GaSe : Gallium Selenide

ZnTe : Zinc Telluride

LT-GaAs : Low-Temperature-Grown GaAs

SI-GaAs : Semi-Insulating GaAs

Si : Silicon

SR : Stanford Research Systems

APT : Advanced Positioning Technology

kHz : Kilohertz (10^3 Hertz)

MHz : Megahertz (10^6 Hertz)

GHz : Gigahertz (10^9 Hertz)

FFT : Fast Fourier Transform

fs : Femtosecond (10^{-15} s)

nm : Nanometer (10^{-9} m)

μm : Micrometer (10^{-6} m)

PC : Personal Computer

E_{THz} : Terahertz Electric Field

e : Electron Charge

ps : Picosecond (10^{-12} s)

W : Watt

n : Refractive Index

METU : Middle East Technical University

CHAPTER 1

INTRODUCTION

Terahertz radiation is an electromagnetic radiation that is defined in the frequency range of 300 gigahertz = 3×10^{11} Hz to 3 terahertz = 3×10^{12} Hz where 1 THz = 10^{12} Hz = 1 ps, λ = 300 μm = 0.3 mm, λ^{-1} = 33 cm^{-1}, 4.1 meV, 47.6 °K that is between the microwave and the infrared regions shown in Fig [1.1] [1,2]. Terahertz radiation is also called submillimeter radiation, terahertz waves, terahertz light, T-rays, T-light, T-lux and THz [2].

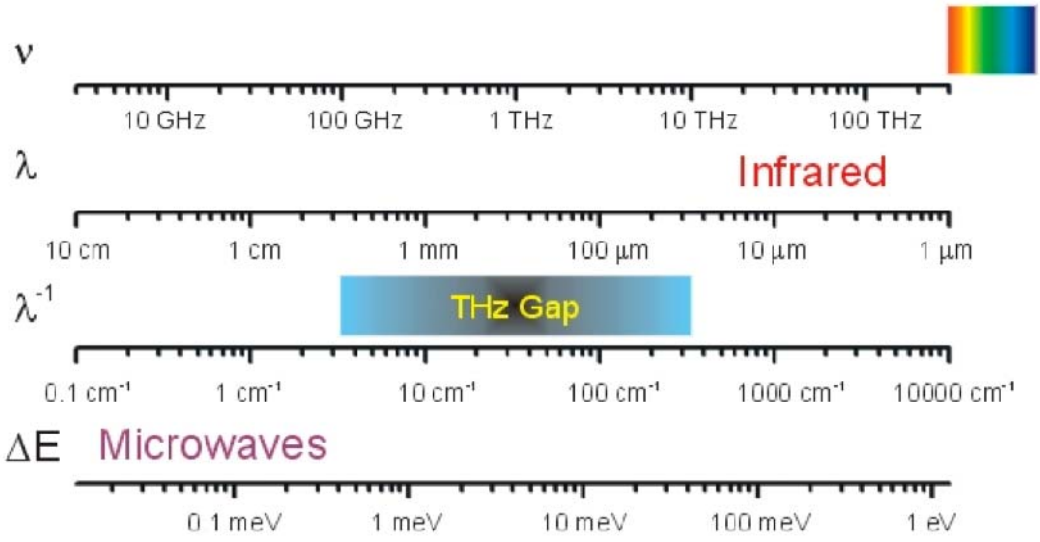

Figure 1.1 THz electromagnetic wave spectrum range [3]

1.1. History of the THz Radiation

Although, in early 1960s, scientists were aware of noticeable advantages of working with the THz radiation, the terahertz technology was not widespread in

science since there were not any adequate radiation sources and suitable detectors. During 1970s, the term 'Terahertz' had been frequently shown in scientific documents and some scientists tried to use microwave and optical techniques in the THz experiments. In 1971, the THz radiation was generated by using nonlinear frequency conversion with an ultrafast laser. In 1976, the THz energy was generated by using optical rectification of short optical pulses [4]. Also, Auston and Cheung were the first implement terahertz time domain spectroscopy in 1985 [5]. In 1988, the first photoconductive antenna was used for such a purpose, which generated and detected the THz radiation between ≤ 100 GHz and ≥ 2 THz. Furthermore, T-Ray imaging process was studied by a research group in 1995 [4].

1.2. Applications of the THz Radiation

Today, the terahertz radiation is commonly used in many areas such as; imaging pills in pharmaceuticals, scientific research conducted in material characterization at universities, and defense related issues for the government.

In commercial areas; T-ray imaging, dentistry (detection of tooth decay), terahertz time domain spectroscopy, medical diagnostics (early detection of skin cancer), pharmaceutical process control (pill inspection) has been implemented to date.

In scientific areas the spectrum is broad but to name a few; astrophysics (remote sensing, heterodyne detectors), chemistry (spectroscopy), environmental sensing (pollution detection), plasma diagnostics and biochemistry (DNA analysis) has all been researched.

In government area; home land security-concealed weapon identification, detection of suicide bombers, biological threat detection, NASA-detection of voids in the space shuttle foam, air force- high rate and secure data transfer, flame analysis (rocket or jet engine burn optimization), army-seeing through sand storms, TSA-passenger screening, hidden weapons detection and contraband detection [6]. In more recent developments, T-ray imaging has gained attention as a substitute for X-ray imaging. There are some reasons for this change. The first one is that

T-rays have lower energy (non-ionizing photons) than X-rays. The second one is that T-rays provide us spectroscopic analysis and identification of the matter as well as imaging the structure [7]. Astrophysicists have utilized T-Rays for remote sensing of various molecules that make-up distant clouds and galaxies. Remote sensing is an important tool for discerning information about the thermal emission lines of light - weight molecules. In the lower THz frequency range, astrophysicists prefer to use heterodyne detectors (instead of homodyne detection due to order of magnitude larger sensitivity) to get the high resolving power and the high spectral resolution that are required for "intra-galactic" and "interstellar" observations. The Terahertz technology is also used in the plasma diagnostics mostly to determine the electron density profile as a function of time and the position in the plasma. The oldest and the most popular THz application are spectroscopy and material analysis. THz spectroscopy allows us to categorize and compile specific spectral line emissions [8]. It is also possible to rapid scan and do gas identification with the use of THz spectroscopy [9]. The spectroscopy technique we use and is widely implemented in labs across the world with access to ultrafast lasers is a spectroscopy technique called "Terahertz Time Domain Spectroscopy." With this method we can detect many different gases (water vapor, methyl chloride and nitrous oxide, molecules which have a net dipole moment) more rapidly and accurately according to their rotational spectra and since coherent detection is possible with THz-TDS [8], by analyzing phase of the terahertz radiation we can deduce the dielectric properties of the various media.

In this thesis, the terahertz time domain spectroscopy (THz-TDS) method of the THz generation and the detection is used to construct a compact time domain spectrometer using the photoconductive dipole antennas for the generation as well as the detection. Emphasis is given toward understanding of the emitted and detected THz power in the system.

1.3. Terahertz Time Domain Spectroscopy (THz-TDS)

THz-TDS set-up is shown in Fig. [1.2]. This set-up uses an ultrafast laser to generate and detect the THz electromagnetic radiation.

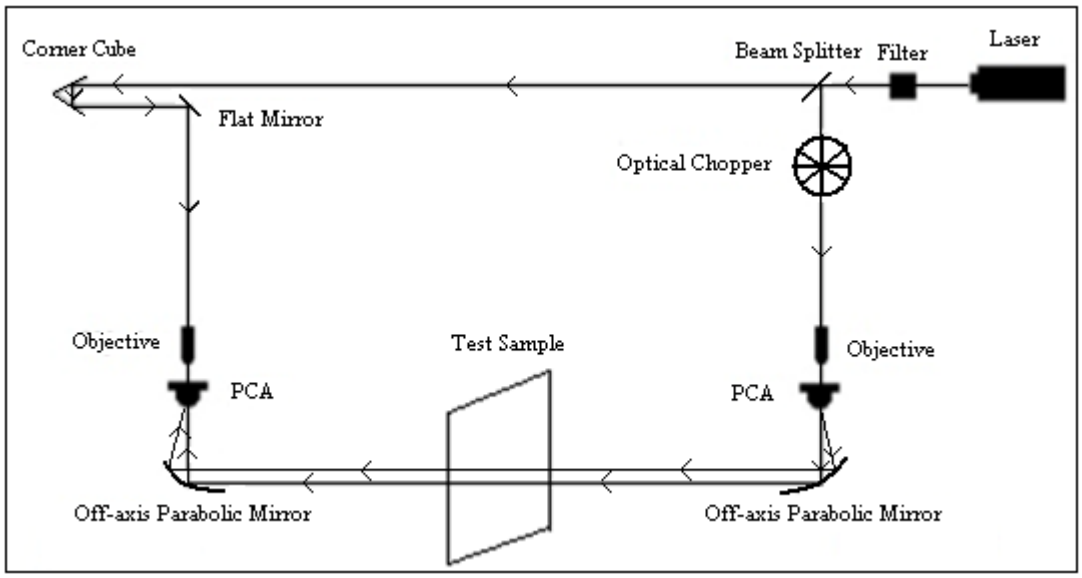

Figure 1.2 Terahertz Time Domain Spectroscopy Set-Up

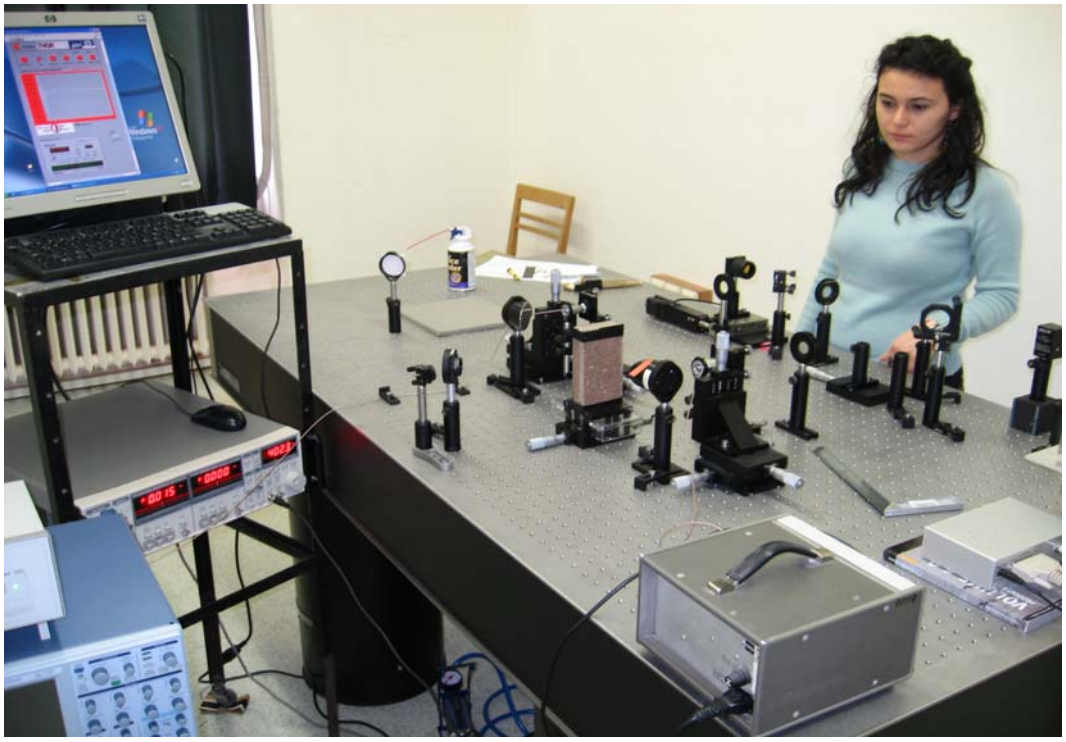

Figure 1.3 A photo of our THz-TDS Set-Up

The THz-TDS is very useful technique to get fundamental structural information about various materials. The set-up is described in detail later. The sample is generally placed in the path of the THz beam, whose properties are analyzed by obtaining a transmission with no sample to that with and then comparing the measurements for differences.

A common point for all terahertz spectroscopy systems is that since the photon energy is about 1 meV we can get important information about the materials without doing any harm. Hence, the THz spectroscopy technology is very suitable for imaging processes instead of X-rays that are known as ionizing radiation [3]. For "in vivo" biological samples since water molecules distort and absorb much of the THz radiation, we can only have images of skin, hair, teeth in other words dried biological samples by using T-ray imaging process [10].

By using this technique, it is also possible to measure the phase of the radiation as well as the electric field amplitude of the detected THz signal. Compared with other spectroscopy techniques in the far infrared, in THz-TDS, detector cooling is not needed in order to obtain better signal-to-noise ratios (SNR). The reason for this is that the peak intensity of the THz pulses is above the thermal background-noise level [11].

There are also other advantages of using THz-TDS. The first advantage is that we can get transmitted and reflected terahertz pulse profile whose phase and amplitude is required for calculation of refractive index and absorption coefficient of the materials. The second advantage is by using the THz-TDS technique; it is possible to do research and analyses on multi-layer samples since the THz pulses are measured in time. The third one is that we have a high spectral bandwidth of the THz waveform, which is important property for compound-chemical identification. Furthermore, photoconductive antenna and electro-optic detection methods called coherent time-gated methods that detect the THz electric field without detecting the beam intensity [10].

On the other hand, there are some disadvantages of using THz-TDS. The first one is that having a small spectral range can cause low resolution in our analysis of

samples. The second one is that due to the low average power (~ 1 μW) of THz pulses spectral information can be lost. Finally, the use of ultrafast lasers makes this tool quite expensive [4].

The THz-TDS technique is mainly composed of two parts, THz generation and THz detection. The first and the main step is to learn how we generate the electromagnetic THz radiation.

1.3.1. Terahertz Generation

To understand the mechanism of the THz generation process fully, we firstly should concentrate on the first component of the system called "pulsed or ultrafast" laser that generates THz electromagnetic pulses and then we can focus on the THz generation methods.

1.3.1.1. Pulsed or Ultrafast Lasers

Pulsed laser is a type of laser that generates pulses at a given repetition rate where each pulse may be as short as 10^{-15} seconds [12]. Pulsed lasers are also known as ultrafast lasers.

Ultrafast laser is a special kind of laser that generates ultrashort pulses (less than 100 picoseconds down to sub-10 femtoseconds) that are broadband electromagnetic pulses with fs time duration. Ultrafast lasers are used in some areas such as micro-machining, femtochemistry, medical imaging where ultrashort laser pulses are used in multi-photon fluorescence microscopes, Terahertz (T-rays) generation and detection, as well as frequency comb techniques due to their large repletion rates from kHz to GHz frequencies [12]. In general, pulsed lasers are commonly used in the THz generation processes especially for THz-TDS. The reasons for using pulsed or ultrafast lasers are to get very high peak powers and to have information about process as quickly as possible which are two important parameters to obtain electromagnetic radiation, which generate THz ultrashort pulses [13]. Mode-locked Ti:Sapphire lasers; diode-pumped lasers, mode-locked fiber lasers and mode-locked diode lasers are some types of ultrafast lasers. Mode-locked lasers are mostly preferred to get ultrashort (sub-ps) pulses [14].

1.3.1.2. Terahertz Generation Methods

Optical rectification, current surge, charge transfer and photoconductive antenna methods are well-known terahertz generation methods. The first three methods have the same underlying physical process called “rectification” [15].

Of the four-generation methods, the photoconductive and the optical rectification are two commonly used ones to generate broadband, ultrashort-pulsed THz beams. In fact, the photoconductive antenna method is the most preferred method for the THz-TD spectroscopy because the photoconductive antennas can convert visible/near-IR pulses to the THz radiation [1] and also that we can get much higher peak THz electric field by using the photoconductive method compared to the one obtained by the optical rectification through difference frequency mixing for THz generation [16]. On the other hand, there is a limitation of using the photoconductive method that because the process of generation takes place slowly due to the resonant characteristics of the antenna and finite lifetime of the generated carriers (electrons and holes) in the detection antenna [17].

In the photoconductive antenna generation method, an ultrashort laser pulse illuminates the photoconductive dipole gap of the antenna. If the laser pulse energy is greater than the band gap energy of the semiconductor, the semiconductor absorbs the energy. Each absorbed photon generates an electron in the conduction band while generating a hole in the valence band. With the help of applied bias voltage to the PC antenna, the photo-excited carriers are accelerated to form transient photocurrent. This generated time-varying transient current radiates subpicosecond electromagnetic THz radiation [11,18,19,20]. Rounding the electrodes of the photoconductive antenna and insulation protection cause an increase in the maximum bias voltage of the antenna and this leads an improvement of the THz radiation intensity [21].

Optical rectification (OR) is another well-known pulsed THz generation method. Yang et al. firstly studied this THz generation method with the use of a $LiNbO_3$ nonlinear optical crystal. However, $LiNbO_3$ nonlinear materials cannot succeed in adequate velocity matching formed as a result of velocity difference between the probe beam (visible beam) and the THz beam. Hence some scientists studied optical

rectification by using other materials such as $LiTaO_3$, GaAs, ZnTe and GaSe [3,4]. Today, ZnTe material is the most commonly used crystal in the optical rectification (as well as electro-optic detection) method. The reason for this is due to the crystal having a sufficient absorption of the visible beam as well as offering an adequate velocity matching between the THz and visible wavelengths [3]. In fact, there are additional criteria to choose the best material to use in both optical rectification and electro-optic detection [22]:

a) The material should be transparent to the laser pulse.

b) The material should contain low attenuation.

c) The static birefringence should be small

The optical rectification method is a second order nonlinear optical process that depends on generating different frequencies to produce much longer wavelengths. In this method, the ultrashort laser pulse is directed to the nonlinear transparent crystal that is easily electrically polarized at high optical intensities and the rapid change in the electrical polarization emits the THz electromagnetic radiation. The radiated field is proportional to the incident photons and the second order susceptibility, $\chi^{(2)}$. Hence, the intensity of the generated THz radiation can be increased by using a crystal with large second order susceptibility. ZnTe crystal with a <110> orientation is the most used one. However, there is a disadvantage of using a ZnTe crystal. When ZnTe is illuminated with a high-power laser pulse, other nonlinear processes like second harmonic generation, two-photon absorption and free carrier absorption can be also seen and these cause a decrease in the intensity of the emitted THz radiation [23]. Although having low output powers, the pulse bandwidth of the THz radiation generated by optical rectification is higher compared to the one generated by photoconductive methods [24].

1.3.2. Terahertz Detection

As well as THz generation, the THz detection process is also very important in developing THz technology. Although an expected THz electromagnetic radiation is generated, we cannot achieve smooth and powerful THz radiation waveforms unless the THz detection process is also adequate. Therefore, it is important to prefer the

best THz generation and complimentary detection process according to the experimental needs. As written in the section [1.3.1.2], we preferred to do the experiment by using photoconductive methods to measure a high peak THz electric field and also peak THz power. Now, it is time to examine the THz detection methods and to understand "Why photoconductive detection methods are more suitable for our experimental needs?"

1.3.2.1. Terahertz Detection Methods

Two commonly used THz detection methods are the photoconductive method and the electro-optic method. Lock-in detection and chopping frequency are two important requirements for both detection methods.

The photoconductive detection method is more efficient at frequencies smaller than 3 THz because of having better signal-to-noise ratio and sensitivity due to the limiting characteristics of the semiconductor material (such as LT-GaAs) [25]. In this detection method, a time-delayed laser pulse is focused onto the photoconductive detection dipole gap to excite the semiconductor material. With the excitation process, electrons and holes are generated. The photo-excited carriers are accelerated by the THz radiation instead of the bias voltage used in the photoconductive generation antenna. These accelerated carriers generate a transient photocurrent and the lock-in amplifier detects the time-varying transient current.

In recent years, the electro-optic detection method has been used more commonly instead of the photoconductive methods because of a higher detection bandwidth and ease of implementation [17].

The electro-optic detection method is also sometimes called "the inverse of optical rectification" [26]. This detection method is not a second order nonlinear optical process as was the case for optical rectification, but it is a linear effect based on the change of index of refraction (birefringence) due to the applied THz electric field.

In the electro-optic method, both the probe beam and the THz beam are focused onto the crystal. We can get maximum signal and the best time resolution if the THz

beam and the probe beam pass through the crystal with the same speed [27]. During the motion of these two beams in the crystal, an electric field is generated that forms a birefringence in the detection crystal. Polarization of the probe beam that travels through the crystal is changed as a result of the induced birefringence [28]. After passing through the crystal, the probe beam is split into two beams by the means of polarizing beam splitter. Two separated beams are focused to the balanced photo-detector to measure intensity difference (ΔI) between them and a signal is detected which is proportional to the THz electric field [29].

In this study, THz waveforms are generated and detected by photoconductive (photoconductive antenna) methods. As mentioned in the section [1.3.2], we use photoconductive method in the generation process to obtain a high peak THz electric field and high peak THz power whereas the photoconductive method is chosen in the detection process to obtain better SNR and sensitivity at the low end of the THz spectrum.

The photoconductive method is based on a photoconductive antenna. In general, photoconductive antennas (PCA) are made of a thin LT-GaAs film, grown on a semi-insulating GaAs substrate (SI-GaAs) and a silicon lens attached to the back of the substrate. The thin film is made of Low-temperature-grown GaAs (LT-GaAs) because it has good carrier mobility, large resistivity and ultrashort carrier lifetime, shorter than 1ps [33,19]. High carrier mobility and large resistivity are two important parameters to have high photon emission radiated from the photoconductive antenna. It is hard to find a material having high carrier mobility and large resistivity at the same time. Hence, a material having large resistivity and good carrier mobility is sufficient. The other parameter, short carrier lifetime, is essential to decrease detector noise of the photoconductive antenna [5]. Because of these three desirable properties, the LT-GaAs is the more commonly used material for photoconductive emitter or detector antenna. SI-GaAs is also a highly resistive material and its carrier lifetime is about 500 ps. The Silicon lens is used to increase the extraction efficiency of the THz waves upon detection and the PCA with Si lens attached upon generation allows for more smooth and powerful THz waveforms as can be examined in Fig. [1.3] and Fig. [1.4] [17]. On the contrary, Si-lens diffracts the generated THz beam and this

causes loss of the THz intensity at the detector end. Another lens or mirror must be located behind the antenna to focus the THz beam and to prevent this loss.

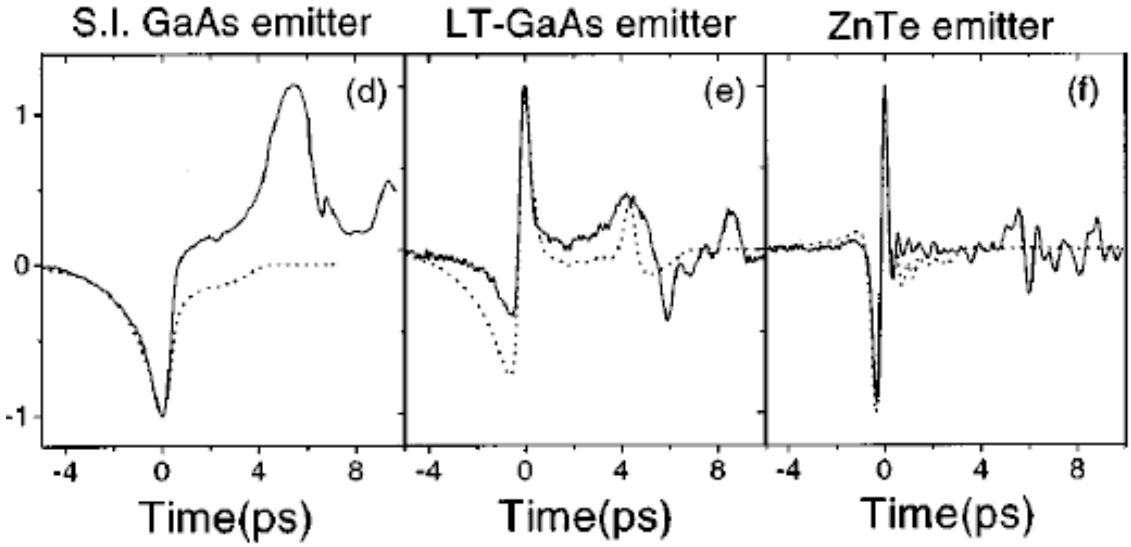

Figure 1.4 The THz waveforms generated the PCA with no substrate lens [17]

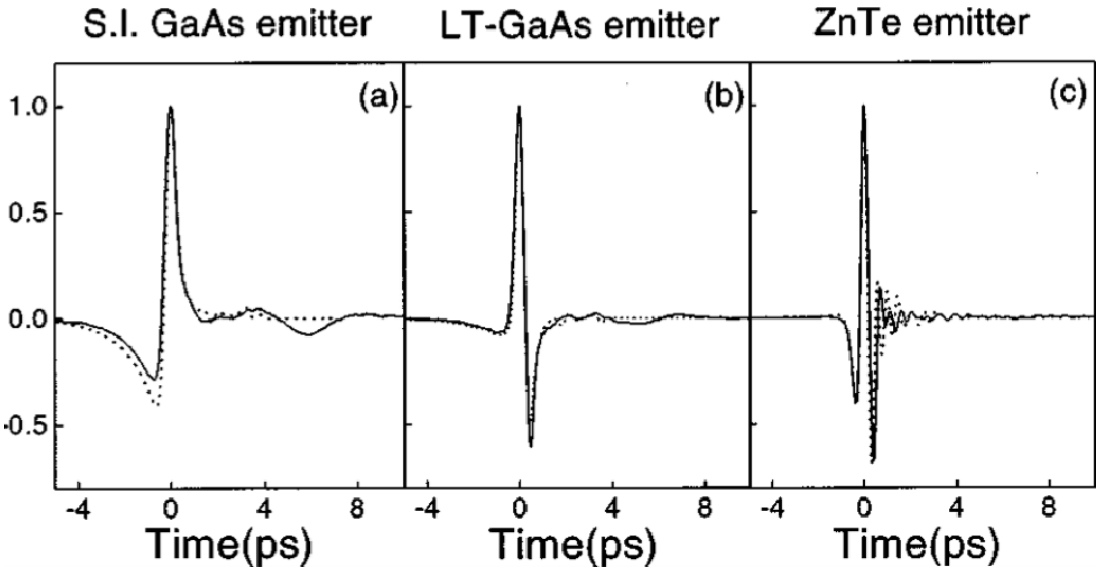

Figure 1.5 The THz waveforms generated by the PCA with substrate lens [17].

CHAPTER 2

THE EXPERIMENT

2.1. Introduction

The experimental set up used for generating and detecting ultrashort THz pulses is shown in Fig. [2.1].

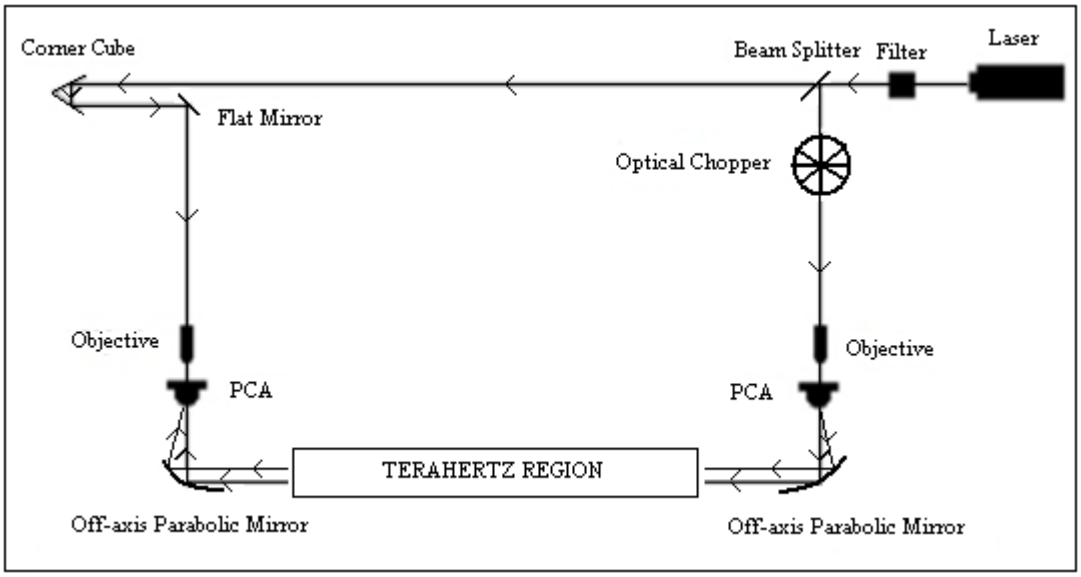

Figure 2.1 The Experimental Set-Up

Our experimental system was either driven by a OneFive GmbH Origami-8 Erbium doped femtosecond fiber laser or femtosource Ti:Sapphire mode-locked laser.

The visible laser beam was sent though a band-pass filter (for the case of the mode-locked Er:doped fiber laser to remove the fundamental component), a beam splitter, an SR540 optical chopper or a function generator to modulate the beam, flat mirrors, objectives to focus the visible beam onto the dipole gap of the photoconductive antenna, and photoconductive antenna (PCAs) obtained from BATOP GmBh. Two 90° off-axis parabolic mirrors were used to collimate the THz beam, a SR830 lock-in amplifier was used to detect the transient current, and a 1" corner cube mirror was used as well as a Thorlabs DC-servo stage to change the time delay of the gating pulse. In addition, a labview program was used to control the system by a personal computer.

The experimental set up is mainly formed by two arms called “generation arm” and the “detection arm”. The optical chopper or the function generator, one of the objectives, the PCAs and the parabolic mirrors are located in the generation arm. The detection arm consists of the stepper stage motor, the corner cube, the flat mirror, the other objective, the PCA, and the parabolic mirror. In order to comprehend the experiment deeply, it is important to get required knowledge about the optical instruments used in the experiment.

2.2. Optical Instruments Used In The Experiment

The origami-8 Erbium doped femtosecond fiber laser properties are a 75 MHz repetition rate, 149 fs duration and 25 mW output power. On the other hand, the Ti:Sapphire mode-locked laser has a 15 fs pulse duration and 75 MHz repetition rate. The femtosecond Er:doped fiber laser has two outputs: infrared (1560 nm, fundamental) and visible (780 nm, second harmonic).

Lock-in amplifiers can detect and measure very small signals in the order of nano-amps or nano-volts at a fixed frequency and phase. By this way, noise signals at other frequencies are blocked and the experiment becomes more precise. The phase of the lock-in reference oscillator must be equal to the phase of signal detected for a precise measurement, which is equal to $V_{sig} = \mathrm{Cos}\,(\theta_{sig} - \theta_{ref})$. By using a second phase sensitive detector this condition is not necessary. This additional phase sensitive detector generates two outputs $X = V_{sig}\,\mathrm{Cos}\theta$ called ‘in phase’

component and Y= V_{sig} Sinθ called 'quadrature' component. When θ is equal to zero, X output measures the signal. In fact, the important condition to remove phase dependency is computing R that is equal to $(X^2+Y^2)^{1/2} = V_{sig}$. If it is necessary, it is possible to calculate the phase, θ between signal and lock-in reference by the following equation [30];

$$\theta = Tan^{-1}(Y / X) \qquad \textit{Equation 2.1}$$

The SR830 lock-in amplifier is one of the more widely used amplifier that has dual phase sensitive detectors and measures X, Y and R without any calculation. The SR830 lock-in amplifier is preferred due to its high stability, greater accuracy and better noise rejection. The amplifier detects signals from 1 mHz to 102 kHz frequency range. "SR" is the abbreviation for Stanford Research Systems that manufactures scientific instruments, test and measurement instruments, time and frequency instruments and vacuum instruments [31].

The SR540 optical chopper can chop frequencies in the range from 4 Hz to 3.7 kHz. The 75 MHz femtosecond fiber laser was used in the experiment and so we chopped the laser beam at 400 Hz. Chopping the laser beam has some limitations. At high frequencies, noise decreases whereas SNR increases. In addition, at some point, the signal decreases too. Moreover, the chopping process decreases the power of the laser beam. To negate this power loss, we used the function generator instead of the optical chopper.

Off-axis parabolic mirrors have some advantages. The first advantage is that it is easy to focus the THz beam to the expected point (minimization of overall system size) by the means of off-axis parabolic mirror. The second advantage is that the system weight can be minimized as a result of using the off-axis parabolic mirror. The last advantage is the minimization of the system cost.

The APT stepper motor is controlled by using a special software program, which can be converted into the main labview program. It is used for controlling the position of the corner cube mirror and subsequently the delay of the gating pulse. Generally, these optic mirrors are made of gold because of high conductivity.

However, the Aluminum made mirrors are mostly preferred in THz studies. The reason is being the low absorption and high reflection properties of aluminum. The corner cube can move a maximum (round trip) 60 μm on the stepper stage. Time duration between the each step is fixed at 0.4 ps because the photoconductive antenna has 2,5 THz bandwidth. Meanwhile, the time duration between the start and the stop positions is about 1000 seconds.

Labview program is the main component of the experiment. It is easy to control the stepper motor, to get the THz pulse graph and the FFT transform of obtained data by the means of prepared labview program as shown in Fig. [2.2].

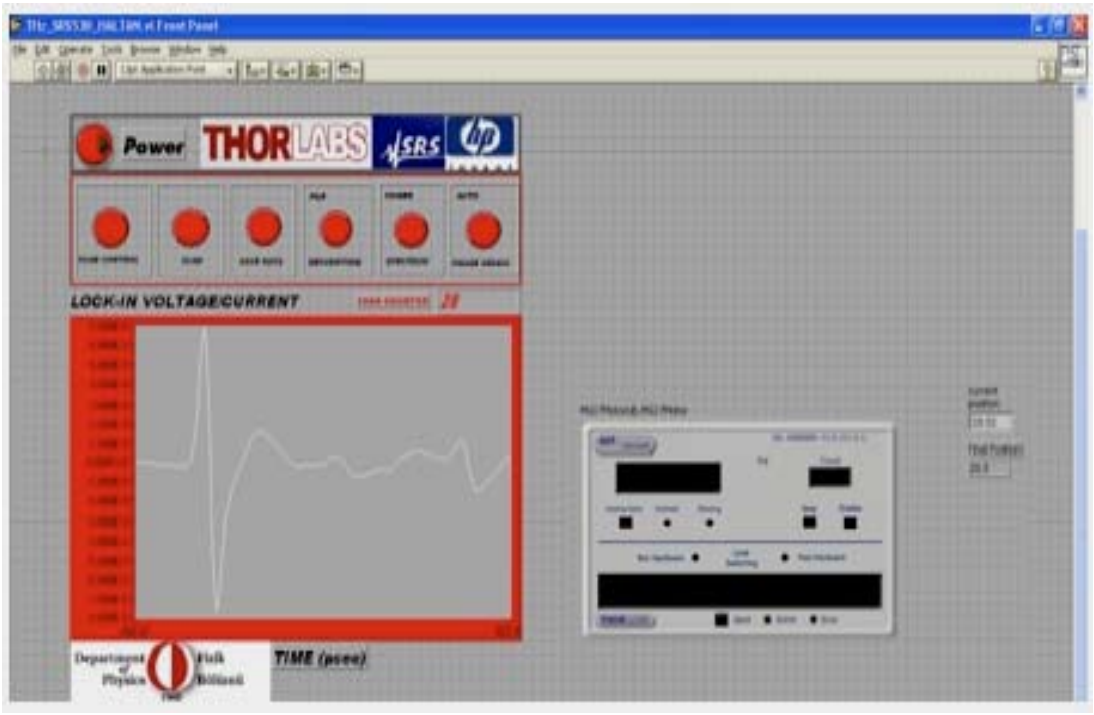

Figure 2.2 THz pulse profile on the labview program

In the experiment, to generate and detect THz pulse, two different shaped-same structured BATOP GmBh photoconductive dipole antennas were used that are the PCA-44-06-10-800 (at 800 nm, 44 μm length, 6 μm dipole gap and 10 μm width) shown in Fig. [2.3] and the PCA-40-05-10-800 (at 800 nm, 40 μm length, 5 μm dipole gap and 10 μm width) shown in Fig. [2.4].

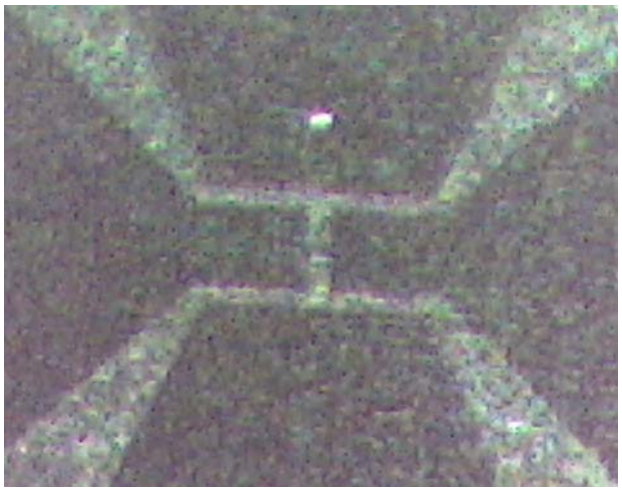

(a)

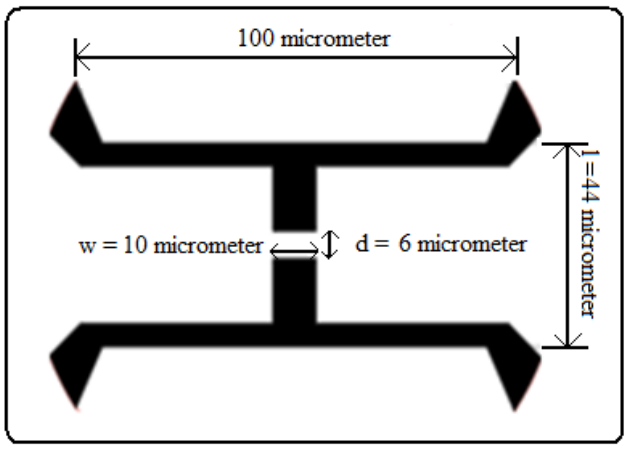

(b)

Figure 2.3 (a) The PCA-44-06-10-800 photo (b) The PCA-44-06-10-800 diagram

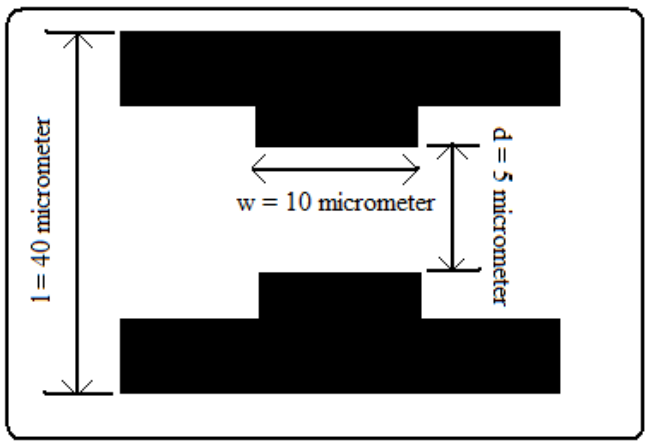

Figure 2.4 The schematic diagram of the PCA-40-05-10-800

Each photoconductive antenna can be used as transmitter and receiver [19,18]. In fact, the PCA-40-05-10-800 is the best for receiver (detection).

The PCA-44-06-10-800 is sensitive to frequencies between 100 GHz and up to 3 THz. Ideal laser excitation wavelength for the antenna is 800 nm and the antenna resonant frequency is 1 THz. We can calculate the resonant frequency of any antenna as follows [32]:

$$\nu_r = \frac{c}{\lambda_r} = \frac{c}{2l_e\varepsilon_e^{1/2}} = \frac{c}{2l_e\left[(1+\varepsilon_d)/2\right]^{1/2}} \qquad \textit{Equation2.2}$$

where;

ν_r = resonant frequency

λ_r = resonance wavelength

c = the speed of light [~ 3×10^8 $m.s^{-1}$]

ε_e = effective dielectric constant

ε_d = dielectric constant of substrate [for GaAs $\varepsilon_d = 13$ and $\varepsilon_e = (1+ \varepsilon_d) / 2 = 7$]

l_e = effective length which is equal to $\{(L+ 2D)^2 + W^2\}^{1/2}$ where L is the length of the antenna , D is the dipole gap , W is the width of the antenna and for the PCA-44-06-10-800 antenna L = 44 μm, D = 6 μm, W = 10 μm and l_e = ~ 56.9 μm, ν_r = ~ 1 THz whereas for the PCA-40-05-10-800 antenna L = 40 μm, D = 5 μm, W = 10 μm and l_e = ~ 51 μm, ν_r = ~ 1.1 THz.

In addition, some electrical parameters are shown in Table [2.1] and some optical excitation parameters are shown in Table [2.2].

Table 2.1 Electrical parameters of the PCA-44-06-10-800 [33].

Electrical Parameters	Minimum Ratings	Standard	Maximum Ratings
Dark Resistance	20 MΩ	25 MΩ	30 MΩ
Dark Current at 10V	300 nA	400 nA	500 nA
Voltage	-	20 V	50 V

Table 2.2 Optical excitation parameters of the PCA-44-06-10-800 [33].

Optical Excitation Parameters	Minimum Ratings	Standard	Maximum Ratings
Excitation laser wavelength	500 nm	800 nm	850 nm
Optical reflectance at 1040 nm	7% at 500 nm	5% at 800 nm	7% at 850 nm
Optical mean power	-	40 mW	200 mW
Optical mean power density	-	100 $kW.cm^{-2}$	500 $kW.cm^{-2}$
Carrier recovery time	-	400 fs	-

The PCA-40-05-10-800 is sensitive to frequencies from 500 GHz up to 5 THz. Ideal laser excitation wavelength is 800 nm and the resonant frequency of the antenna is 1.1 THz. Some electrical parameters of the antenna are shown in Table [2.3] and some optical excitation parameters are shown in Table [2.4].

Table 2.3 Electrical parameters of the PCA-40-05-10-800 [33].

Electrical Parameters	Minimum Ratings	Standard	Maximum Ratings
Dark Resistance	20 MΩ	25 MΩ	30 MΩ
Dark Current at 10V	3 μA	4 μA	5 μA
Voltage	-	20 V	50 V

Table 2.4 Optical excitation parameters of the PCA-40-05-10-800 [33].

Optical Excitation Parameters	Minimum Ratings	Standard	Maximum Ratings
Excitation laser wavelength	500 nm	800 nm	850 nm
Optical reflectance at 1040 nm	32 % at 500 nm	7 % at 800nm	8 % at 850 nm
Optical mean power	-	40 mW	200 mW
Optical mean power density	-	100 $kW.cm^{-2}$	500 $kW.cm^{-2}$
Carrier recovery time	-	200 fs	-

2.3. The Experimental Set-Up

At the beginning of the set-up procedure, two optical irises with the same height were placed in front of the laser at intervals and the laser was aligned. We put power meter in front of the femtosecond fiber laser and measured the power of the beam (both visible and infrared) as 69.8 mW. After being sure that the laser passes through

in a straight line, a filter was located in front of the laser to transmit through the 780 nm beam and to eliminate 1560 nm beam. This time, we put the power meter behind the filter and measured light power (780 nm) as 3.7 mW. Then we changed the filter with another one and got 4.1 mW. Hence, we decided to use the second filter. The following process is to set the beam splitter. The beam splitter was placed behind the filter and the laser light was split into two in order to create the generation arm and the detection arm shown in Fig. [2.1]. The power in the generation arm after the beam splitter was ~ 15 mW and the power in the detection arm after the beam splitter was ~ 46.6 mW (without filter). The next procedure was to locate the optical chopper in the generation arm after the beam splitter. We set the chopper to ~ 400 Hz to eliminate other effects like incandescent lights (50 Hz and its harmonics) and connected the chopper to the lock-in amplifier. After that we placed a photo-detector, connected to the lock-in amplifier, in the position where the antenna would be located later and tried to find the maximum photon position (0.260 mV at 1×10 sensitivity in channel A on the lock-in amplifier). Immediately, a pinhole on a translation stage was placed in position after the pinhole and the photo-detector controlled maximum photon location was found (0.160 mV at lock-in). Afterwards, a 20 mm objective on a controller stage was fixed into a position between the chopper and the pinhole very close to the pinhole and again the maximum photon location was detected (~ 0.08 mV). The major procedure was to place the PCA-44-06-10-800 antenna connected to the function generator (supply ±15 AC V to the antenna) into the position of the pinhole and we tried to decrease the resistivity of the antenna to ~ 0.89 MΩ (at the stage position x = 2.25 mm, y = 7.36 mm, z = 2.75 mm) by very small positional changes of the antenna. After setting all the optical instruments in the generation arm, it was time to set the optical instruments in the detection arm as shown in the Fig. [2.1].

To construct the detection arm, the first step was adjusting the corner cube in the system. The corner cube was placed on a stage connected to the stage motor. We tried to arrange the incident beam and the reflected beam at the same height. The reflected beam direction was changed into another direction called the detection arm, parallel to the generation arm by the means of a flat mirror. An iris was located after the flat mirror in the detection arm. By moving the corner cube forward and

backward on the stage, we checked the beam direction and deduced that it did not shift. Then, the power meter was located at a position behind the flat mirror in the detection arm and we measured the laser beam power as ~ 9.20 mW (without the filter). After making sure that the beam was in a straight line, we placed the photo-detector at the position parallel to the generation photoconductive antenna and tried to find the maximum photon location (~ 108 mV at 2 × 100 sensitivity channel A on the lock-in amplifier). After that, the pinhole on another controller stage was fixed to this position and then again the maximum photon location was found after the pinhole (~ 60 mV). The second objective on a translation stage was placed between the flat mirror and the pinhole very close to the pinhole and the maximum photon position was found again (~ 70 mV). Afterwards the other PCA-44-06-10-800 was put at the position of the pinhole. Later on, we achieved to decrease resistivity of the detection antenna to 0.63 MΩ (at stage position x = 3.39, y = 14.64, z = 21.16). The last and the hardest step was adjusting the off-axis parallel mirrors in the experimental set-up. To locate the parabolic mirrors, another high intensity laser was used. Firstly, we placed one of the parabolic mirror at a position distance from the generation antenna as much as the focal length of the mirror (f = 7.8 cm) and the other parabolic mirror was located at a position distance from the detection antenna as much as the focal length of the mirror (f = 7.8 cm). Secondly, we focused the laser on the hyper-hemispherical silicon lens of the generation antenna and checked whether the shape of the beam reflected from the parabolic mirror had a circular shape or not. If not, we moved the parabolic mirror until we got a circular shape. After achieving circular shape with the reflected beam, we checked whether this beam fell on the other parabolic mirror. We moved this parabolic mirror, which is mounted on a translation stage, until the circular reflected beam covered whole of the parabolic mirror. Then, we checked that two intersecting reflected beams coming from parabolic mirrors were focused on hyper-hemispherical silicon lens of the detection antenna. If not, we moved the parabolic mirror until having this focus. After all these procedures were done, we removed the high intensity laser from the system and the set-up was completed.

While moving the DC motor translation stage forward and backward by hand, we tried find the THz pulse peak. After being sure that the THz pulse was being

generated, we controlled the motorized stage with the help of the labview program. To obtain data, we executed the labview program on the PC and pushed the scan control button. Four boxes (inputs) are shown on the program front screen called start, stop, step and wait time as shown in Fig. [2.5].

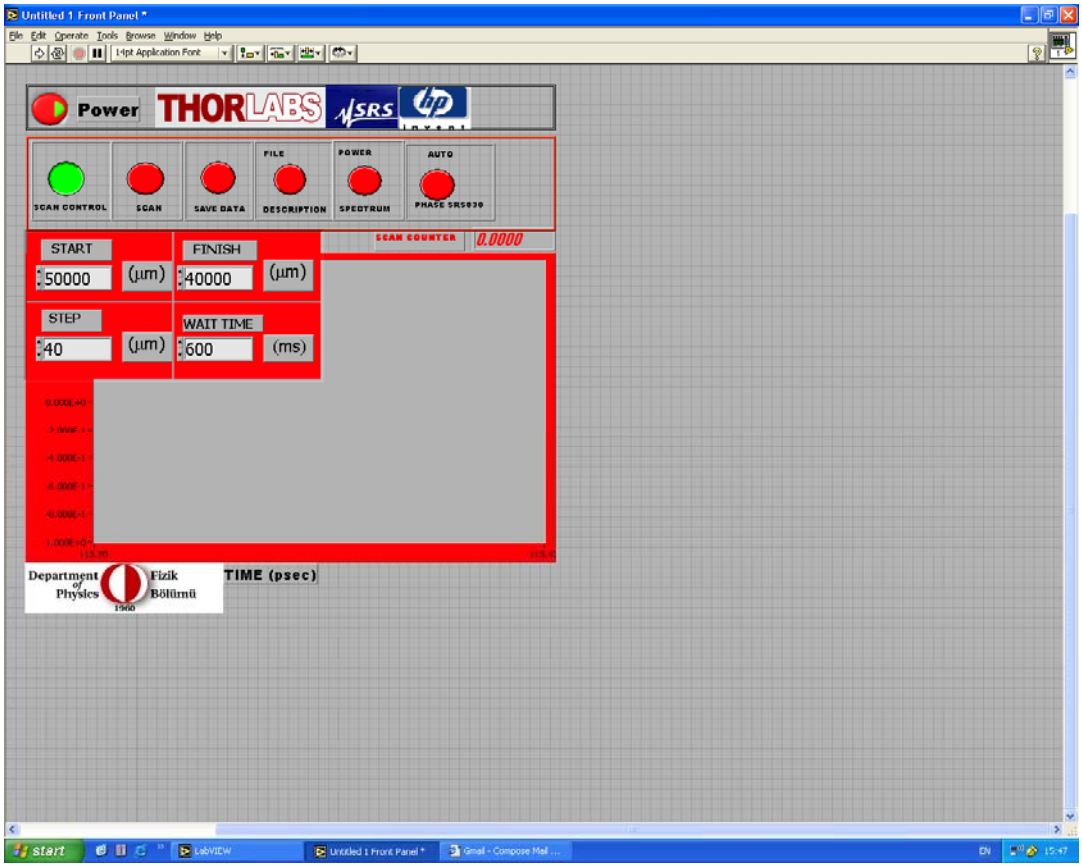

Figure 2.5 The APT stepper motor control by the labview program

First of all, the required start-stop positions are written in the start and the stop boxes. Then, the delayed time, which is ~ 600 ms, is written in the wait time box and the step size is written in the step box before we run the program. We calculated the step size of the motor in the following way. We multiplied the distance, which we want to go forward with the stepper motor, by 2 because of the beam return. Then, we divided this number by 300 µm because 1 ps = 300 µm (using the speed of light) and got the step size of the motor.

While running the program, we acquire the THz pulse profile and the FFT spectrum of the THz pulse. To get Fourier transform of the THz pulse we must have 2^n data. When the program is completed, we get data points greater than 1024. Hence, we ignore excess data and use the Origin graphical analysis software to plot and analyze the data. Noticeably, the THz pulse profile has a 3.47 ps pulse width. The time-domain waveform and the FFT transform of the THz pulse are shown respectively in Fig. [2.6] and Fig. [2.7].

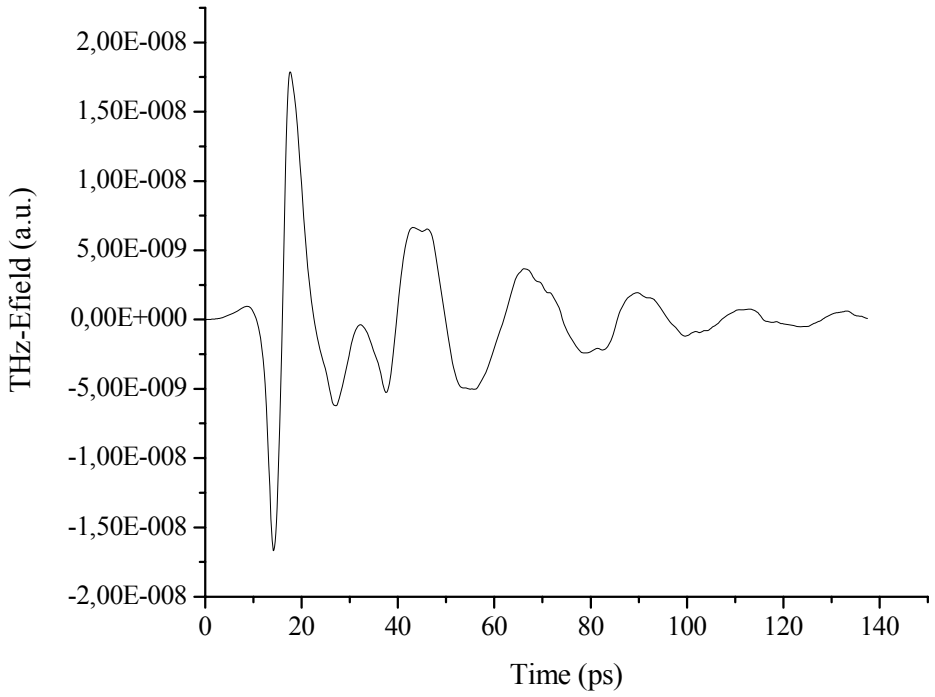

Figure 2.6 The THz waveform that generated by the photoconductive antenna for the Er:doped femtosecond fiber laser

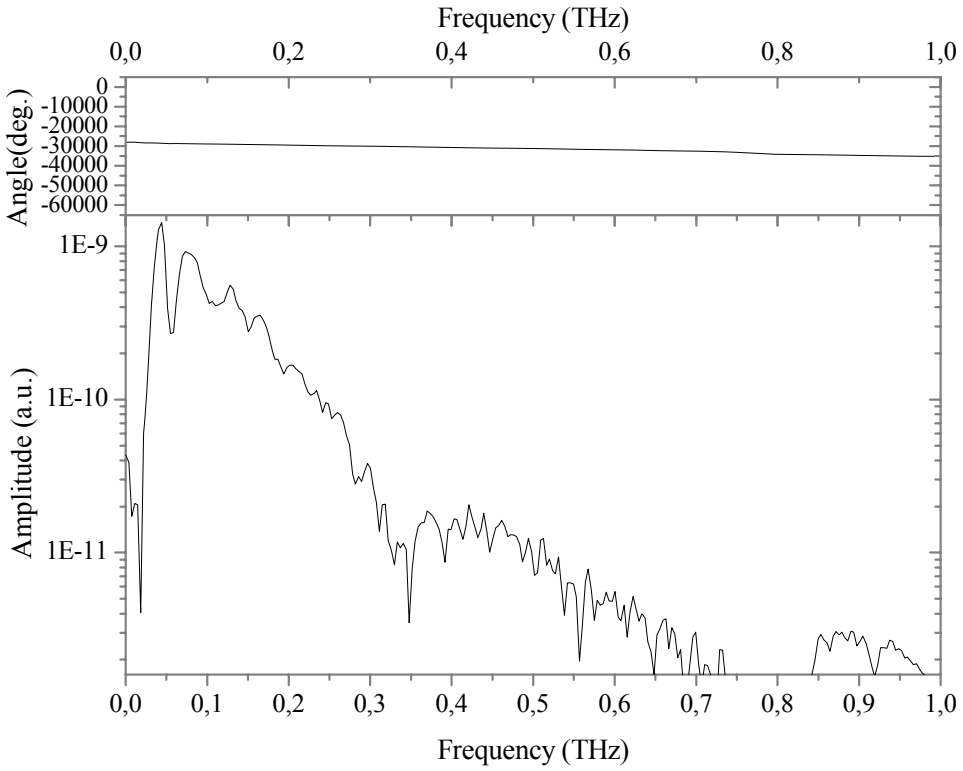

Figure 2.7 The Fourier spectrum of the THz pulse that shown in Fig. [2.6]

We did the same experiment by using the Ti:Sapphire mode-locked laser, the PCA-40-05-10-800 as the detection antenna, two 40 mm-objectives and two 62.5 mm 90° off-axis parabolic mirrors (Melles Griot, f = 11.68 cm).

In this experiment, we chopped the pump laser beam at 2,5 kHz to decrease the noise in the signal and applied a ± 15 V AC bias voltage between the electrodes of the generation photoconductive antenna. Then, we increased the value of the applied voltage to ± 30 V and to ± 35 V DC (while using an optical chopper of the same frequency, roughly 2.5 kHz) and realized an increase in the THz pulse profile. As a result of this, we concluded that the strength of the generated THz pulse is directly proportional to the bias voltage value applied to the generation antenna like that shown in Fig. [2.8] [19].

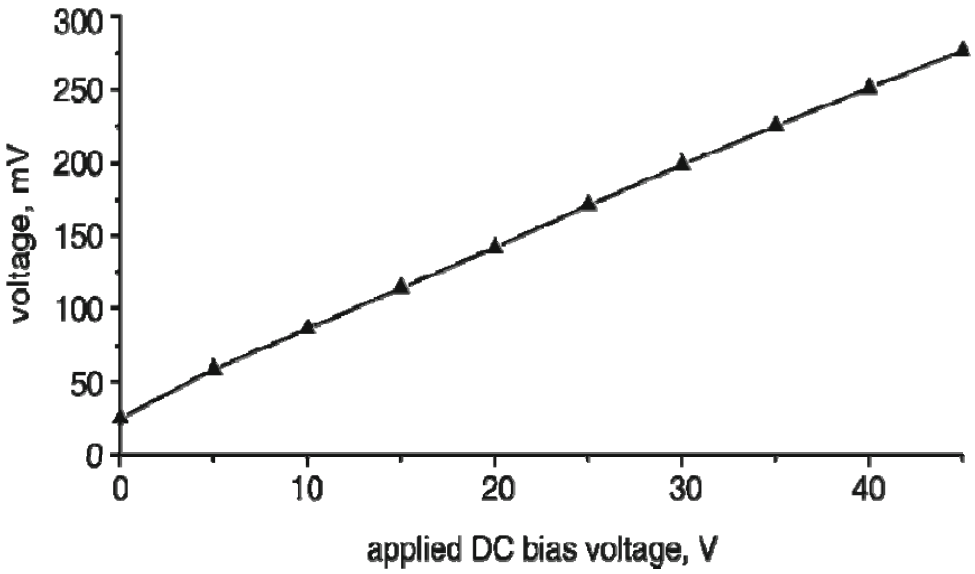

Figure 2.8 Dependency of the output voltage of detection antenna to bias DC voltage applied to generation antenna [19]

On the contrary, the THz pulse profile does not directly depend on the laser spot size and the pumping power as shown in the Fig. [2.9].

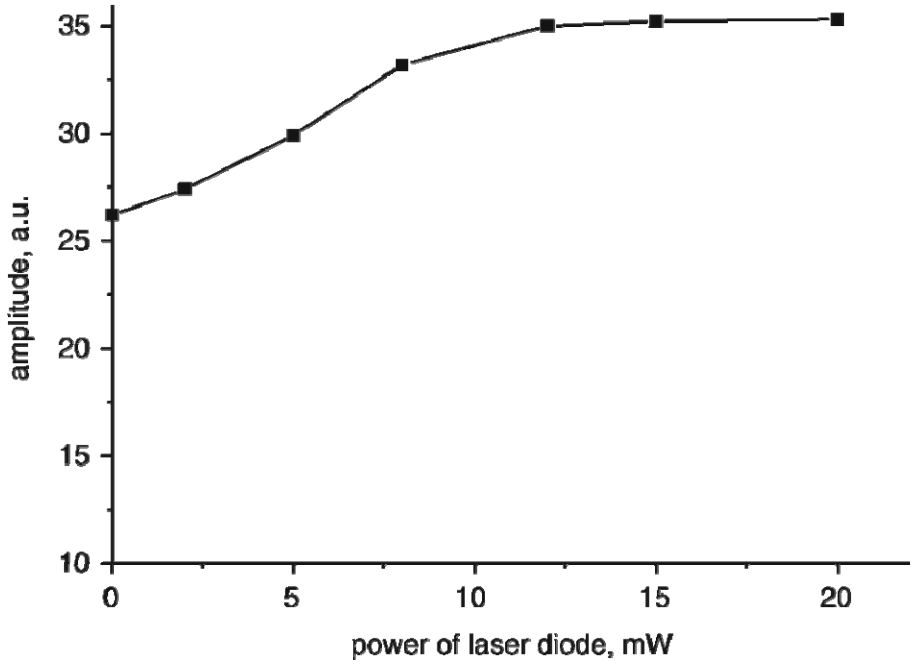

Figure 2.9 THz peak amplitude as a function of pump power of laser [19]

In fact, the intensity of the THz pulse is determined by the LT-GaAs material properties in the photoconductive antenna [19].

After optimizing the system with the Ti:Sapphire ultrafast laser, one of the best obtained THz pulse graphs is shown in Fig. [2.10] and also the FFT of the THz pulse is shown in Fig. [2.11] (at Mode-Locked Power = 280 mW, Chiller Temperature = 18.63 °C, Resistance $_{\text{generation antenna}}$ = 256 kΩ and Resistance $_{\text{detection antenna}}$ = 100 kΩ, both off-axis parabolic mirrors located at an optimized distance of 10.5 cm from the antenna). We obtained a 2.13 ps pulse width in the time domain and roughly a bandwidth ~ 1 THz.

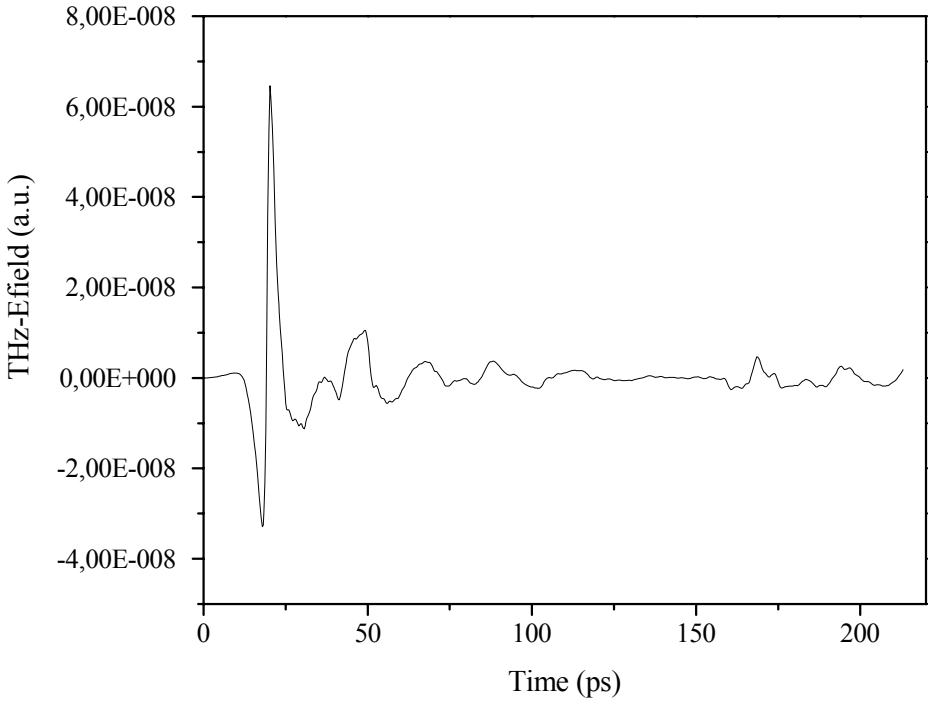

Figure 2.10 The THz pulse profile generated by using the Ti:Sapphire mode-locked laser

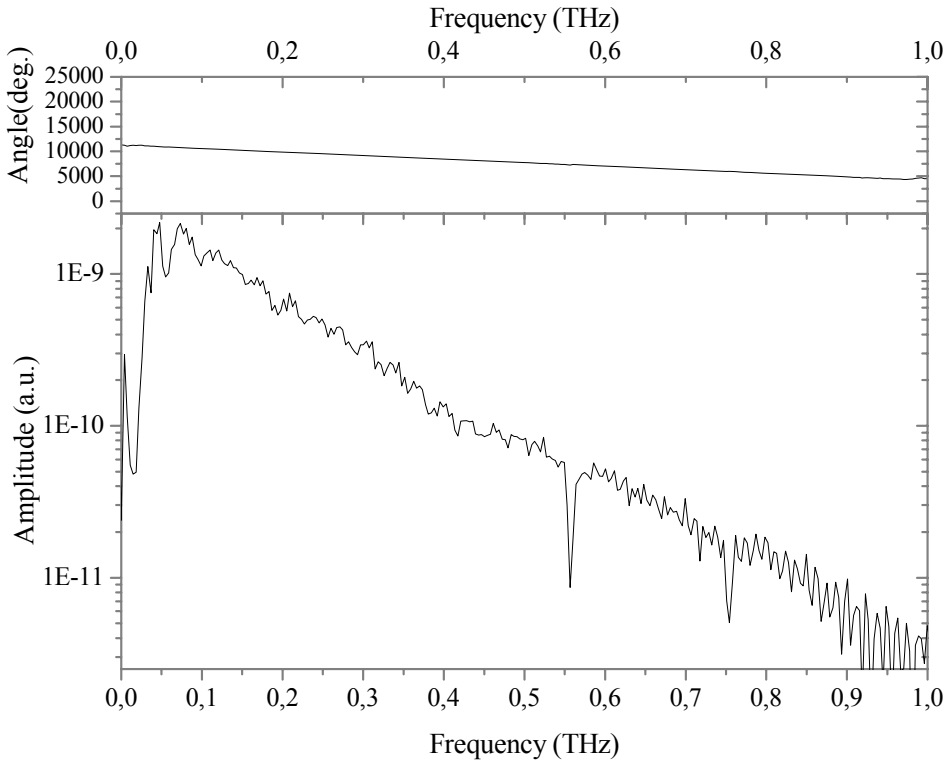

Figure 2.11 The FFT spectrum of the THz pulse profile shown in the Fig. [2.10]

2.3.1. Example Measurements (Soil Transmission)

We also analyzed some soil samples by examining their THz transmission. We wanted to understand the scattering and transmission properties of various dry and wet soils. To do this we obtained the THz pulse transmission and the FFT transform shown in Fig. [2.12] by placing an empty box, a box filled with soil in Fig. [2.13] and a box filled with wet soil shown in Fig. [2.14] independently between the parabolic mirrors (in THz region) and observed the changes in the THz pulse profile.

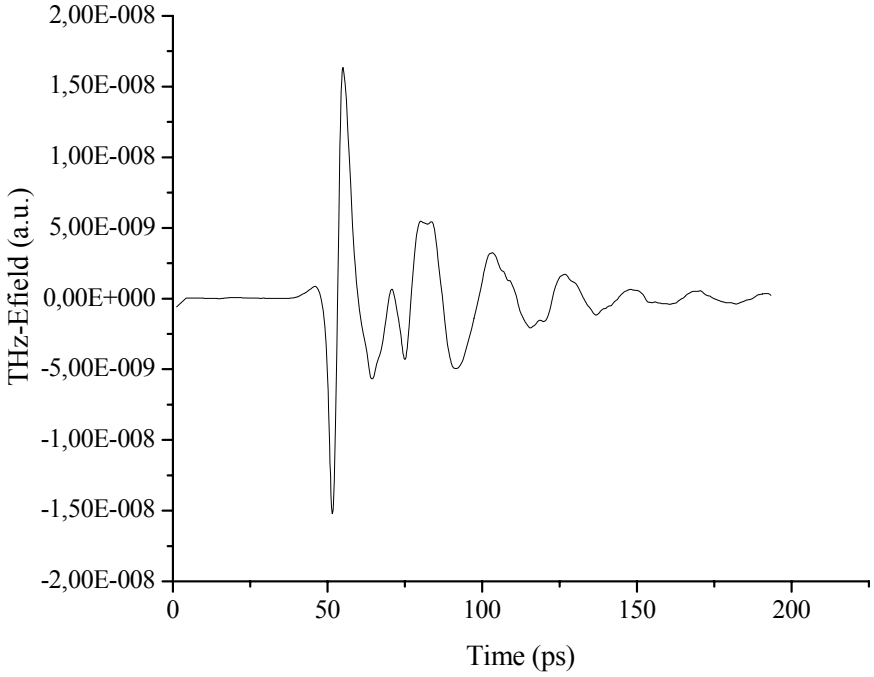

(a)

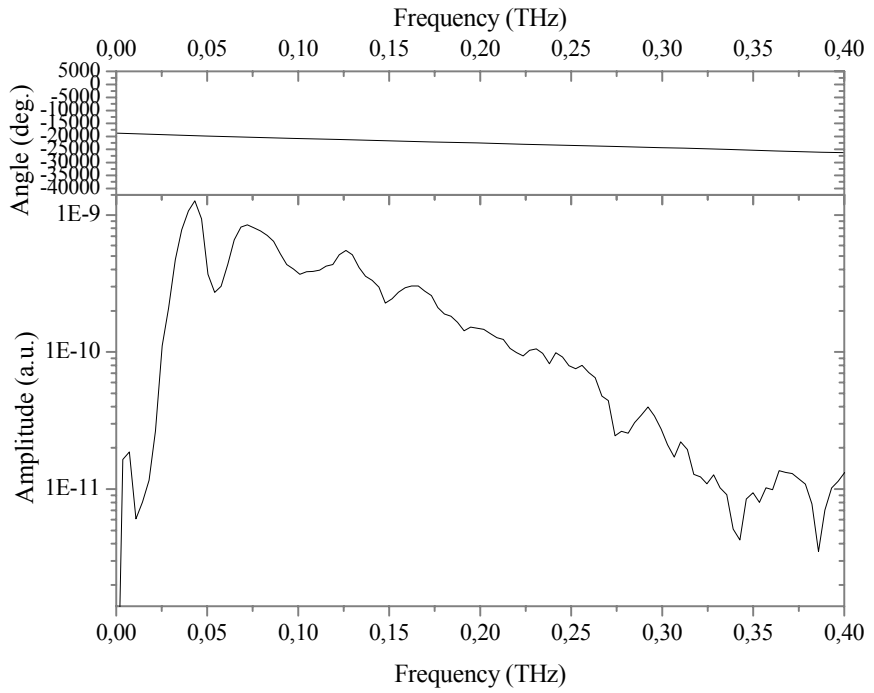

(b)

Figure 2.12 (a) The THz pulse graph of empty box (b) FFT transform of empty box

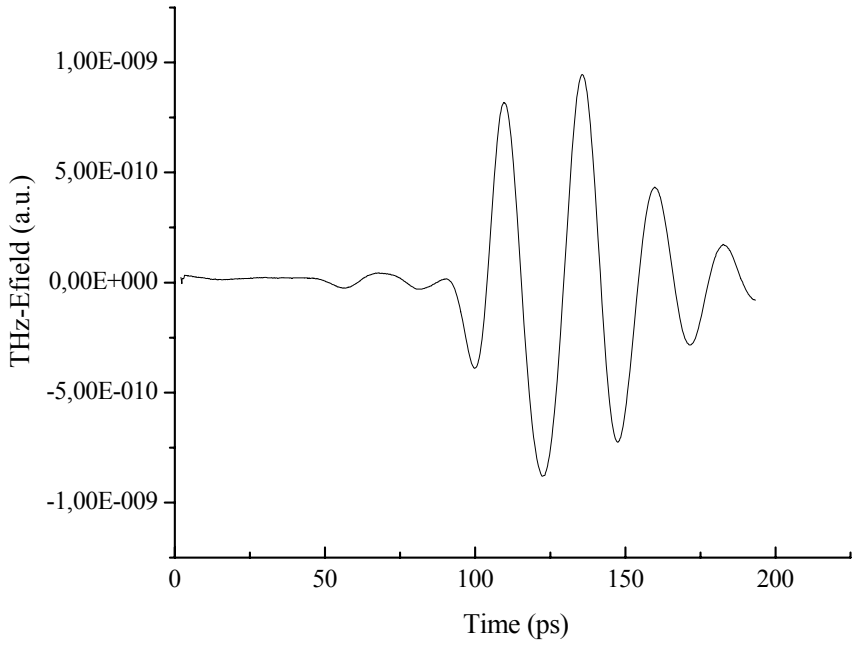

(a)

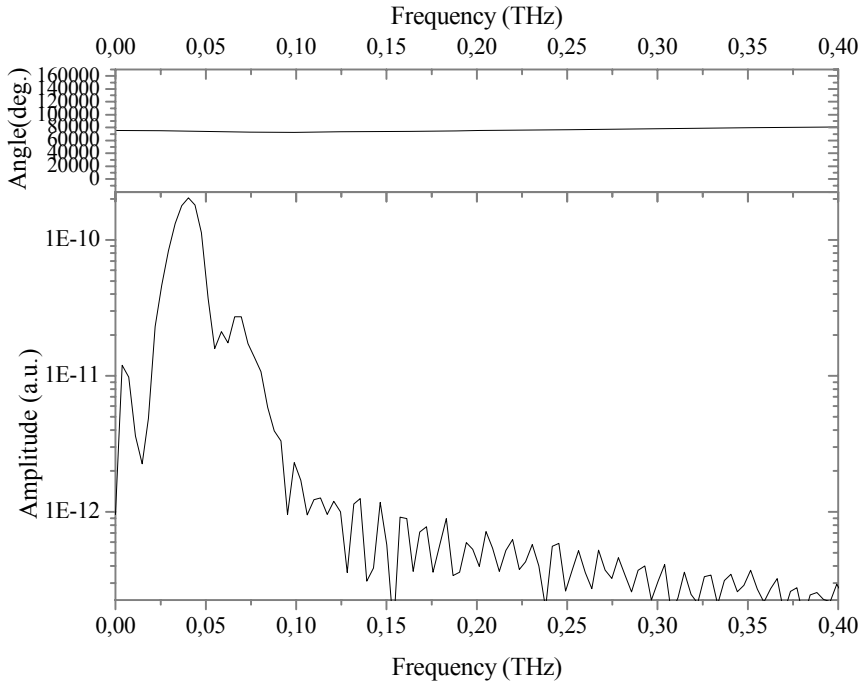

(b) FFT transform of soil filled box

Figure 2.13 (a) The THz pulse graph of soil filled box (b) FFT transform of soil filled box

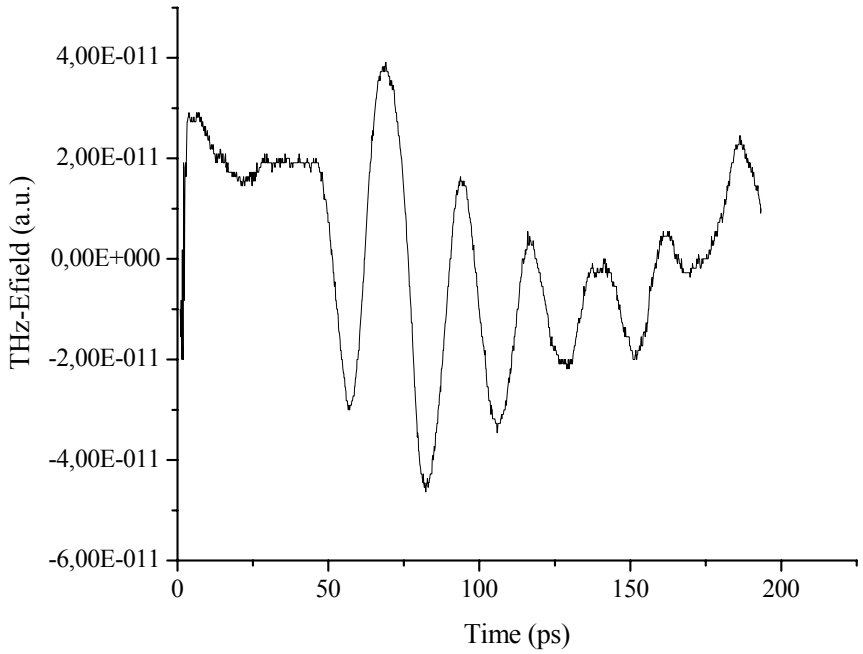

(a)

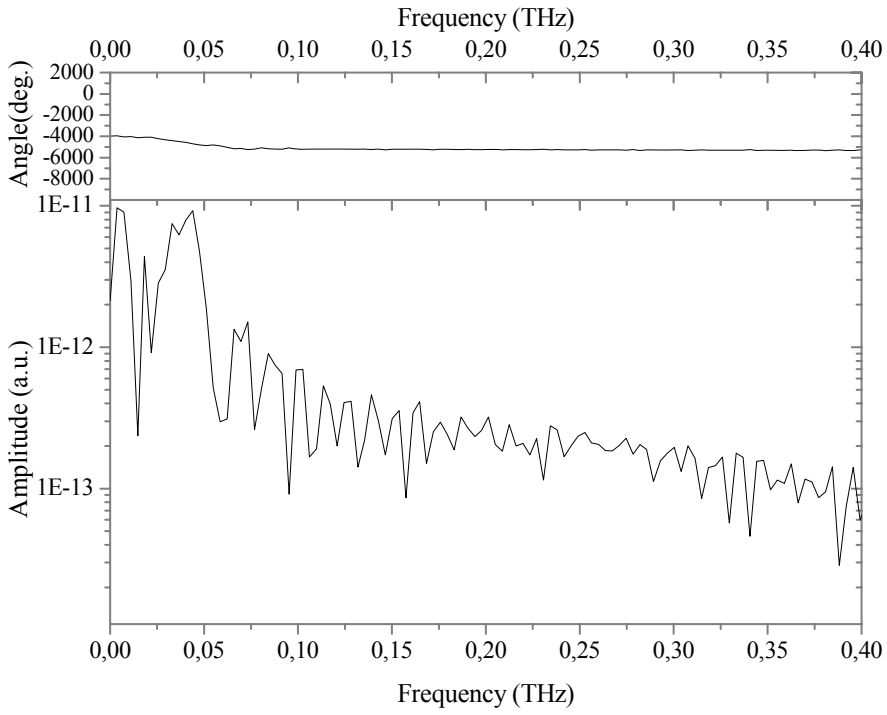

(b)

Figure 2.14 (a) The THz pulse graph of wet soil filled box (b) FFT transform of wet soil filled box

As shown in Fig. [2.12.a], the THz could pass through the empty box without any changes in the THz pulse profile. There was only a change in the position of the THz pulse because of the refractive index of the box. The THz was also able to pass through the soil filled box and the wet soil filled box with a change in the pulse profile as a result of the absorption and dispersion. In fact, any materials except non-polar and non-metallic can absorb the THz pulse [4]. Water (polar) molecules in wet soil absorbed the THz and the pulse profile was extremely attenuated. Hence, it is important to eliminate humidity and liquid water from the environment in which we expect to transmit the THz pulse. It is possible to decrease the absorption effect of water vapor by placing all the optical instruments into an evacuated box [11] or nitrogen purged box. The strength of the absorption mainly depends on the absorption coefficient of for each material that can be calculated by D'Alambert's law as follows [47]:

$$\alpha(r) = -\frac{1}{d} ln \frac{I_1}{I_0} \qquad \textit{Equation2.3}$$

where;

α_r = absorption coefficient

d = thickness of the sample

I_0 = intensity before passing through the sample

I_1 = intensity after passing through the sample.

The absorption coefficient formula is also represented as [34]:

$$\alpha(r) = \frac{2 \cdot \nu \cdot n \cdot k}{c} \qquad \textit{Equation 2.4}$$

where;

ν = frequency of the light in vacuum

n = refractive index of the medium

k = attenuation index or the extinction coefficient of the material

c = the speed of light

CHAPTER 3

POWER CHARACTERIZATION

It is possible to measure the value of the THz power directly by using a bolometer. The bolometer is an optical instrument that measures the power of the electromagnetic radiation by the means of temperature change in the medium. This means that generated time-varying transient current changes the temperature of the surrounding medium and as a result this change in the temperature is detected by the bolometer [35]. In addition, typical bolometer for THz detection is more sensitive to the wavelengths in the range 200 μm - 1 mm and this means that the bolometer is sensitive to both the light and ambient thermal effects. The most important disadvantage of using the bolometer is that when we use the bolometer in the experimental set-up, we must cool it by liquid Helium [16]. Therefore, without using a bolometer our only choice to get information about the generated and detected THz power is by way of a theoretical calculation and approximation.

There are different types of theoretical calculation methods to obtain the THz power in a THz-TDS system. The Hertzian dipole approximation and the induced open-circuit voltage methods are two well-known calculation methods among them. Hence, we concentrated on the two methods and compared the results.

3.1. THz Power Calculation by the Hertzian Dipole Approximation

Dipole antenna presented in Fig. [3.1] is an antenna that made of a straight wire fed at its center by radio waves (AC voltage). After developing by Heinrich Rudolph Hertz in 1886, the dipole antenna has been also called as “Hertzian Dipole Antenna” [36].

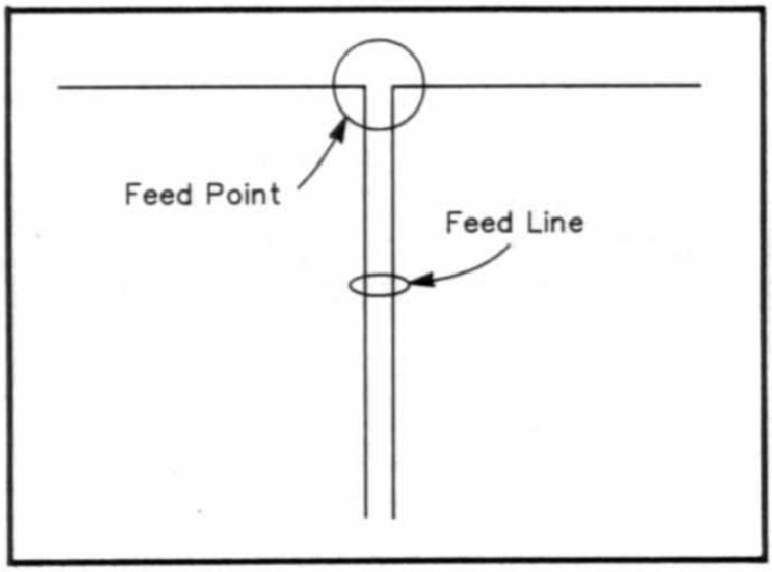

Figure 3.1 A simplest dipole (Hertzian) antenna [37]

If the length of the dipole antenna is in the range of $l < (\lambda / 50)$, this antenna is called as short dipole antenna shown in Fig. [3.2] [38].

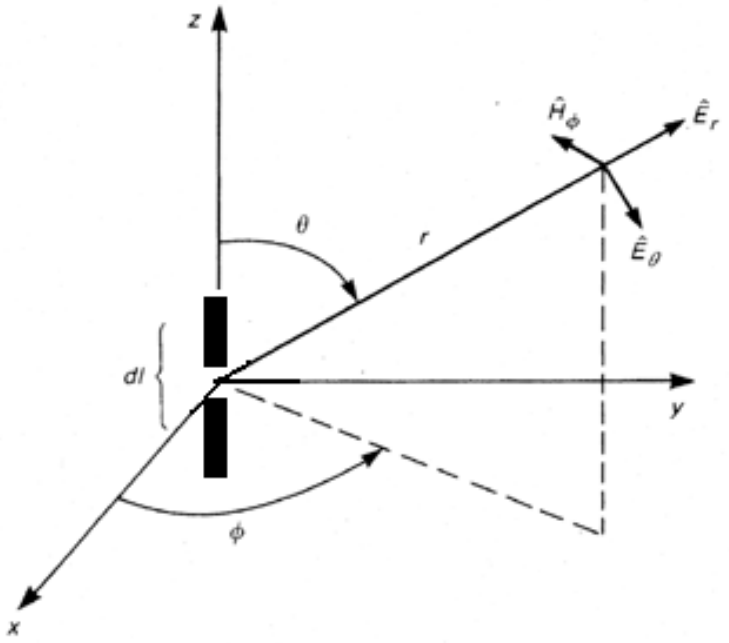

Figure 3.2 A simple Hertzian Dipole diagram [50]

In the Fig. [3.2], d is the dipole gap of the antenna, dl is infinitesimal length of the antenna in z-direction, E_r is the radial component of electric field, E_θ is the angular component of electric field, H_Φ is the azimuthal component of magnetic field, r is the distance from the center of the dipole length to the point and θ is the angle between the dipole direction to the radial distance.

As mentioned before, in the photoconductive method, the time-varying current, which is generated as a result of the excitation process of the photoconductive antenna dipole gap, radiates electromagnetic THz radiation. To obtain the THz power, first we calculate the electric field strength of the generated THz pulse.

We concentrate on the THz electric field in the far field from the antenna, which is a distance much greater than the wavelength, which is about 300 microns. In our experiment this approximation is valid since the detector antenna was at least 30 - 40 cm away from the generation antenna.

The THz radiation electric field in the far field of the PCA can be represented as [32,10]:

$$E_{THz}(r,t) = \frac{l_e}{4\pi\varepsilon_0 c^2 r}\frac{\partial i(t)}{\partial t}Sin\theta = \frac{l_e A}{4\pi\varepsilon_0 c^2 r}\frac{\partial J(t)}{\partial t}Sin\theta \quad \textit{Equation 3.1}$$

where;

l_e = effective length of the dipole

A = area of the dipole

ε_0 = dielectric constant of the air

c = the speed of light

i(t) = time-dependent current

θ = angle from the direction of the dipole shown in Fig. [3.2]

J(t) = the surface current density

We can conclude from the equation [3.1] that

$$E_{THz} \propto \frac{\partial J(t)}{\partial t} \qquad \textit{Equation 3.2}$$

Hence, to calculate the THz radiation electric field, it is important to get a relation of time-varying surface current density [18,10].

$$J = en\upsilon_h + (-e)n\upsilon_e \qquad \textit{Equation 3.3}$$

where;

e = charge of the electrons and the holes

n = carrier charge density

υ_h = velocity of the holes

υ_e = velocity of the electrons

Then, the equation for the far-field radiation pattern can be written as [10, 18, 39, 40]:

$$E_{THz} \propto \frac{\partial J(t)}{\partial t} \propto e\upsilon \frac{\partial n(t)}{\partial t} + en\frac{\partial \upsilon(t)}{\partial t} \qquad \textit{Equation 3.4}$$

where;

$\upsilon = \upsilon_e - \upsilon_h$

According to the equation [3.4], we can conclude that [10]:

a.

$e\upsilon\frac{\partial n(t)}{\partial t}$ component of the current density is much stronger than the second component of the current density, $en\frac{\partial \upsilon(t)}{\partial t}$. Hence, we can ignore the second one.

b.

E_{THz} pulse width is directly proportional to the pulse width of the used laser beam.

c.

The value of the E_{THz} is also depends on the used antenna structure.

The surface current density is also written as [32,10,41]:

$$J(t) = e\mu E_b n(t) \qquad \textit{Equation 3.5}$$

where μ is mobility of the substrate (for LT-GaAs μ ~ 200 $cm^2.V^{-1}.s^{-1}$), E_b is the bias electric field that equal to V_b (the applied bias voltage) / d (the dipole gap of the PCA), n (t) is time-varying carrier density which is equal to $n_o e^{-\frac{t}{\tau_c}}$ where n_o is the carrier density at t = 0, τ_c is the carrier lifetime of the substrate (for LT-GaAs τ_c ~ 0.3 ps)

If we take the first time derivative of the equation [3.5], we get:

$$\frac{\partial J(t)}{\partial t} = e\mu E_b \frac{\partial n(t)}{\partial t} \text{ where } \frac{\partial n(t)}{\partial t} = -\frac{1}{\tau_c} n_0 e^{-\frac{t}{\tau_c}} = -\frac{1}{\tau_c} n(t) \qquad \textit{Equation 3.6}$$

When we put the equation [3.6] into the equation [3.1], we obtain:

$$E_{THz}(r,t) = -\frac{Ae\mu l_e E_b}{4\pi\varepsilon_0 c^2 r \tau_c} n(t) Sin\theta \qquad \textit{Equation 3.7}$$

In the experiment used the Origami-8 Erbium doped femtosecond fiber laser:

A = the area of the generation antenna (10 μm × 1 μm = 10^{-11} m^2)

e = 1.6 × 10^{-19} C

μ = ~ 200 $cm^2 .V^{-1}.s^{-1}$ = 2 × 10^{-2} $m^2 .V^{-1}.s^{-1}$

l_e = effective length of the generation antenna (~ 56.9 μm)

E_b = 30 V / 6 μm = 5 × 10^6 $V.m^{-1}$

ε_0 = 8.85 × 10^{-12} $C^2.N^{-1}.m^{-2}$

c = 3 × 10^8 $m.s^{-1}$

τ_c = ~ 0.3 ps = 3 × 10^{-13} s

n(t) = time-varying carrier density

To solve the equation [3.7], first of all, we should calculate the time-dependent carrier density generated by the laser according to following equation [3.8]. If we assume that each photon generated one carrier (Quantum efficiency = ~ 1), then:

$$n(t) = n_o e^{-\frac{t}{\tau_c}} = \frac{E_{Pulse}}{E_{Photon}} e^{-\frac{t}{\tau_c}} \qquad \textit{Equation 3.8}$$

For the femtosecond fiber laser, the carrier density is calculated as:

$$n(t) = \frac{\frac{15mW}{75MHz}}{\frac{6.63\times10^{-34}m^2.kg.\ s^{-1}\ \times3\times10^{8}\,m.s^{-1}}{780nm}} e^{-\frac{150\ fs}{0.3\ ps}} \qquad \textit{Equation 3.9}$$

$$= \frac{2\times10^{-10}W.s}{2.55\times10^{-19}m^2.kg.s^{-2}} e^{-0.5} = 4.76\times10^{8} \qquad \textit{Equation 3.10}$$

We need the value of the carrier density in volume. Therefore, we divide the result in the equation [3.10], 4.76×10^8, by the volume of the generation antenna, which is equal to 60 $\mu m^3 = 6 \times 10^{-17}\ m^3$ and then we obtain n (t) / V = $7.93 \times 10^{24}\ m^{-3}$.

After calculating all the values into the equation [3.7], the result is that "$E_{THz} \cong 24.06\frac{Sin\theta}{r}$ N / C". This electric field is the peak electric field value of the THz pulse.

In the experiment used the Ti:Sapphire mode-locked laser, all values of the parameters in the equation [3.7] is the same with the experiment done by using the fiber laser except the time-varying carrier density.

If we calculate the time-varying carrier density for the Ti:Sapphire mode-locked laser by using the equation [3.8], we obtain:

$$n(t) = \frac{\frac{\sim 10mW}{75MHz}}{\frac{6.63\times10^{-34}m^2.kg.s^{-1}\times3\times10^{8}\,m.s^{-1}}{780nm}} e^{-\frac{15\ fs}{0.3\ ps}} = 4.97\times10^{8} \qquad \textit{Equation 3.11}$$

With knowing the volume of the generation antenna is 60 $\mu m^3 = 6 \times 10^{-17}\ m^3$, we can easily calculate the carrier density per unit volume as n (t) / V = $8.29 \times 10^{24}\ m^{-3}$.

When we calculate all the results in the equation [3.7], we get the peak THz electric field generated by the Ti:Sapphire mode-locked laser that is equal to $\cong 25.15\frac{Sin\theta}{r}$ N / C.

After obtaining the peak value of the THz electric field from the analysis onward of equation 3.7, we can easily calculate the peak power of the THz pulse.

As we know that the total radiated THz power [38,42] without considering the loss is:

$$P_{rad} = \iint \left|\vec{P}\right| r^2 d\Omega = \iint \left|\vec{P}\right| r^2 Sin\theta d\theta d\Phi \quad \textit{Equation 3.12}$$

where $\vec{P}$ is the time-average poynting vector that amplitude is equal to $\frac{1}{2}\varepsilon_0 c\left|\vec{E}_{THz}\right|^2$ in terms of the THz electric filed where ε_0 is permittivity of the air (8.85×10^{-12} $C^2.N^{-1}.m^{-2}$) and c is the speed of light ($\sim 3 \times 10^8$ $m.s^{-1}$).

As seen in the equation [3.12], we, firstly, find the value of the time-average poynting vector.

For the Er:doped femtosecond fiber laser according to the result obtained from the equation [3.7]:

$$\left|\vec{P}\right| = ½ \times 8.85 \times 10^{-12} \times 3 \times 10^8 \left(24.06\frac{Sin\theta}{r}\right)^2 \cong 0.77\frac{Sin^2\theta}{r^2} \quad \textit{Equation 3.13}$$

When we put the result shown in the equation [3.13] into the equation [3.12], we get:

$$P_{rad} = 0.77\iint \frac{Sin^2\theta}{r^2} r^2 Sin\theta d\theta d\Phi = 0.77\iint Sin^2\theta\left(Sin\theta d\theta d\Phi\right) \textit{Equation3.14}$$

where the integral equation, $\iint Sin^2\theta(Sin\theta d\theta d\Phi)$, is defined as the solid angle of the generation antenna pattern like shown in Fig. [3.3].

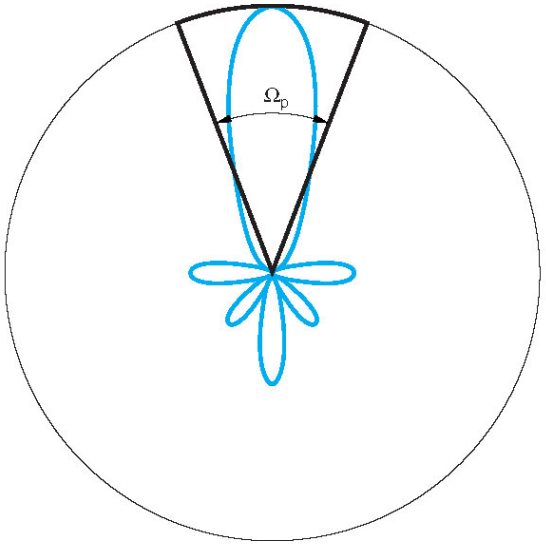

Figure 3.3 The solid angle structure of the antenna [42]

When we calculate the solid angle integral, we obtain:

$$\Omega_p = \iint Sin^2\theta d\Omega = \int_0^{2\pi}\int_0^{\pi} Sin^2\theta(Sin\theta d\theta d\Phi) = \frac{8\pi}{3} \quad \textit{Equation 3.15}$$

After putting the result from equation [3.15] into the equation [3.14], then we get the value of the total radiated peak THz power generated by the THz-TDS system driven by the Er:doped fiber laser as:

$$P_{power}^{peak} = 6.4W \quad \textit{Equation 3.16}$$

In addition, we can also calculate the average power of the generated THz beam by using the femtosecond fiber laser in the Fig. [2.6] as follow:

$$P_{power}^{average} = P_{power}^{peak} \times Pulse\text{-}Width \times Repetition\text{-}Rate \quad \textit{Equation 3.17}$$

where the peak THz power is 6.4 W shown in the equation [3.16], the pulse width is 3.47 ps and the repetition rate of the laser is 75 MHz. Then, we obtain the average THz power as:

$$P_{power}^{average} = \sim 1.7\ mW \qquad \textit{Equation 3.18}$$

The time-average poynting vector of the THz pulse generated by the Ti:Sapphire mode-locked laser according to the result obtained from the equation [3.7] is:

$$\left|\vec{P}\right| = ½ \times 8.85 \times 10^{-12} \times 3 \times 10^{8} \times (25.15 \frac{Sin\,\theta}{r})^{2} = 0.84\ \frac{Sin^{2}\theta}{r^{2}} \qquad \textit{Equation 3.19}$$

The total radiated peak power of the THz pulse generated by the Ti:Sapphire mode-locked laser is (7.03 W) almost the same as the one in the equation [3.16] and the average power of the THz pulse generated by the Ti:Sapphire mode-locked laser is:

$$P_{power}^{average} = \sim 1.12\ m\ W \qquad \textit{Equation 3.20}$$

where the peak power is 7.03 W, the pulse width is 2.13 ps and the repetition rate of the laser is 75 MHz.

The two obtained average THz powers are (1.7 mW and 1.12 mW) higher than the expected values and there can be some reasons of this contradiction. For example; we assume that each photon generates one carrier whereas there is a possibility that some photons cannot generate carries. In addition, we did not take into account power losses as a result of absorption and refraction effects.

3.2. THz Power Calculation by Induced Open-Circuit Voltage

The open-circuit voltage method is the second commonly used one in the THz power measurements. Hence, we can also calculate the THz power by the means of open-circuit voltage, V_{OC}, shown in Fig. [3.4], which represents the receiving antenna circuit layout.

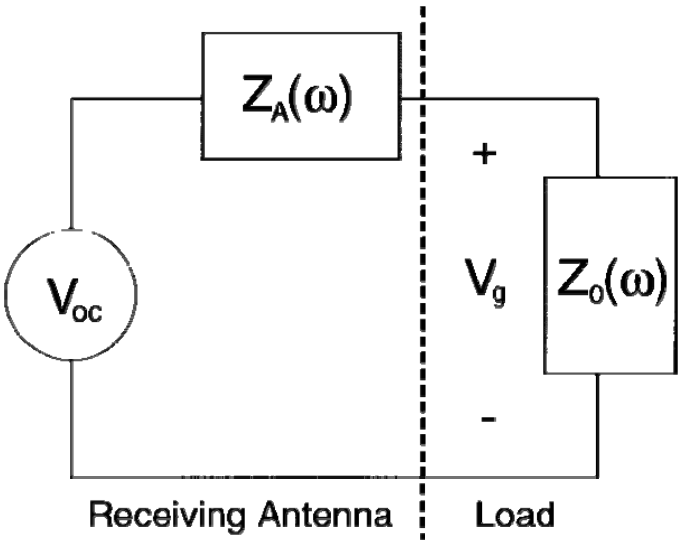

Figure 3.4 An equivalent circuit diagram of an antenna in receiving mode [42]

In the Fig. [3.4] Z_0 is the transmission impedance, Z_A is the antenna impedance and V_{OC} is the induced open-circuit voltage.

To calculate the peak THz power and the average THz power, first of all, we should find a relation between the induced open-circuit voltage and the THz electric field. Hence, we use the reciprocity theorem and obtain a relation at a specific frequency:

$$Z_A(\omega) = Z_0^*(\omega) \qquad \textit{Equation 3.21}$$

where the antenna is connected to the load.

After providing the impedance-matching condition shown in the equation [3.21], we can write a relation between the transmitted power and the receiver power as following [43]:

$$W_r = \frac{\lambda^2 g_{dr} g_{dt}}{(4\pi r)^2} W_t \qquad \textit{Equation 3.22}$$

where;

W_t = transmitted power

λ = wavelength of the THz pulse

r = the distance between the transmitter and the receiver

g_{dr} = directional gain of the receiver

g_{dt} = directional gain of the transmitter

Knowing that the incident THz intensity is equal to $I_{inc} = \frac{|E_{THz}|^2}{2\eta}$ where η is the impedance of free space (~ 377 Ω) and it is also defined as $W_t\left(\frac{g_{dt}}{4\pi r^2}\right)$, we can rewrite the equation [3.22] and we obtain:

$$W_r = \frac{\lambda^2 g_{dr}}{4\pi} W_t\left(\frac{g_{dt}}{4\pi r^2}\right) = \frac{\lambda^2 g_{dr}}{4\pi}\frac{|E_{THz}|^2}{2\eta} \qquad \textit{Equation 3.23}$$

On the contrary, the average power of the load can be defined as [43]:

$$W_r = \frac{1}{8}\frac{|V_{oc}|^2}{R_r} \qquad \textit{Equation 3.24}$$

where R_r is the radiation resistance of the receiving (detection) antenna.

When we put the equation [3.24] into the equation [3.23], then we obtain:

$$|V_{oc}|^2 = \frac{2\lambda^2}{\pi} g_{dr} R_r \frac{|E_{THz}|^2}{2\eta} \qquad \textit{Equation 3.25}$$

For a short dipole antenna g_{dr} is equal to 3 / 2 and for a short monopole that is one half of the dipole, radiation resistance is given by $R_r = 10\pi^2 [l / \lambda]^2$ where l is the length of the detection antenna dipole, which is much smaller than the quarter-wavelength [44,48,49].

After substituting the g_{dr} and the R_r values into the equation [3.25], then we get a relation between the induced open-circuit voltage and the THz electric field as:

$$\left|V_{oc}\right|^2 = \frac{30\pi l^2}{\eta}\left|E_{THz}\right|^2 \qquad \textit{Equation 3.26}$$

We know that the induced open-circuit voltage, V_{OC}, is equal to $I_{THz} \times R_{detection\ antenna}$. When we put the value of induced open-circuit voltage into the equation [3.26], then we can easily obtain value of the THz electric field.

In the experiment done by using the femtosecond fiber laser;

I_{THz} (peak to peak) = 1×10^{-9} A - 3.44×10^{-8} A in range (measured value)

$R_{detection\ antenna}$ = 0.63 MΩ (measured value)

l = 44 μm

$V_{oc} = 6.3 \times 10^{-4}$ V - 0.02 V in range

$E_{THz} = 0.29\ V.cm^{-1}$ - $9.09\ V.cm^{-1}$ in range

In the experiment done by using the Ti:Sapphire mode-locked laser;

I_{THz} (peak to peak) = 1×10^{-9} A - 9.8×10^{-8} A in range (measured value)

$R_{detection\ antenna}$ = 100 kΩ (measured value)

l = 40 μm

V_{oc} = 1 × 10^{-4} V - 9.8 × 10^{-3} V in range

E_{THz} = 0.05 V.cm^{-1} - 4.9 V.cm^{-1} in range

We can calculate the average THz power for the both used lasers according to another form of the time-average pointing vector formula written in equation [3.27].

$$P = \frac{1}{2} c\varepsilon_0 \left|E_{THz}\right|^2 An \qquad \textit{Equation 3.27}$$

where;

c = the speed of light

ε_0 = permittivity of the air

E_{THz} = terahertz electric field

n = refractive index of the GaAs at 1 THz that is equal to ~ 3.2

A = area of circular shape focused beam that is equal to πr^2 where π is 3.14 and r is the radius of the focused beam that is equal to $\frac{\lambda}{4}$ (λ is approximated according to the Rayleigh Criterion which accept that 1 THz = 300 μm and for GaAs substrate $\lambda_n = \lambda / n_{GaAs}$ = ~ 80 μm for 1 THz [44])

Then, for the fiber laser the average power of the THz beam is in the range of 71.8 nW - 70.54 μW (λ = 320 μm for 0.25 THz) whereas for the Ti:Sapphire mode-locked laser the average power of the THz beam is in the range of 0.53 nW – 5.12 μW (λ = 160 μm for 0.5 THz).

CHAPTER 4

RESULTS AND DISCUSSION

In the experiment, we generated THz radiations by the means of photoconductive antenna detection method. Two different laser sources are used in the experiment that are the Er:doped femtosecond fiber laser (149 fs, 75 MHz) and the Ti:Sapphire mode-locked laser (15 fs, 75MHz) . With the use of fiber laser, we obtained ~ 0.25 THz radiation (3.47 ps pulse width) like shown in the Fig. [2.6] whereas we got ~ 0.5 THz radiation (2.13 ps pulse width) by using the Ti:Sapphire mode-locked laser like shown in the Fig. [2.10]. According to these results we have greater THz radiation with the mode-locked laser. The main reason for this small change is the used photoconductive antenna (PCA-40-05-10-800) in the detection arm of the experiment done by using mode-locked laser because this antenna structure is more efficient for detection processes [33] as compared to the PCA-44-06-10-800 antenna used in the detection arm of the experiment done by using the fiber laser.

In fact, our main reason for doing these experiments is to characterize THz power outputs for both laser sources. For theoretical measurements, we mainly used two different types of methods “Hertzian Dipole” and “Open-Circuit Voltage”. Hertzian dipole method which is used for calculation of THz peak electric field, THz peak power and THz average power according to the transmitted radiation (in the generation arm) whereas we calculated THz electric field, and THz average power by using open-circuit voltage method according to the received radiation (in the detection arm). All these theoretical results obtained from the two methods are represented in Table [4.1] clearly.

Table 4.1 Radiated THz peak electric field, radiated THz peak power and average power value of photoconductive antennas for both used laser sources

	Er: doped Femtosecond Fiber Laser		**Ti:Sapphire Mode-Locked Laser**	
	HD[a] Method	OCV[b] Method	HD Method	OCV Method
$\mathbf{E}_{\mathbf{THz}}$	24.06 Sinθ/r	0.29 – 9.09 $V.cm^{-1}$	25.15 Sinθ/r	0.05 – 4.9 $V.cm^{-1}$
$\mathbf{P}_{\mathbf{peak\ power}}$	6.4W		7.03W	
$\mathbf{P}_{\mathbf{avg.\ power}}$	1.7 mW	71.8 nW - 70.54 μW	1.12 mW	0.54 nW – 5.12 μW

[a]HD means the "Hertzian Dipole", [b]OCV means the "Open-Circuit Voltage".

Firstly, let's we analyze the results obtained by Hertzian dipole approximation method. As shown in the Table [4.1], when we calculated THz powers according to the equation [3.7] of Hertzian dipole method we got ~ 1 mW average powers for both lasers and this result is very high for our expectations. Because when we examined some articles including experiments that instruments are very similar to the ones in our experimental set-up, we noticed that they have ~ average THz beam powers in nW or μW range [45]. For example, M. Tani and et al., did their experiment by the means of 80 fs - 82 MHz - 780 nm Ti:Sapphire mode-locked laser, PCA-30-05-20, PCA-20-05-10, PCA-10-05-20 dipole antennas, 15 mW pump power and 30 V bias voltage and they obtained 0.34 μW, 0.12 μW and 0.07 μW THz radiation powers [33]. In addition, some scientists have 38 nW, 10 nW with 5 - 10 mW pump powers after doing their experiments [25]. As a result we found out that the reasons of this excess in calculations can be ignoring absorption effects, reflection loss is ~ 30% at normal incidence [46] and accepting each photon generates one carrier whereas there is a possibility that some photons cannot generate

carries. Moreover, all the results in the table [4.1] for Hertzian dipole method are approximately equal to the each other although we used two different types of laser source. This is possible because peak THz beam is directly proportional to the pump power and the biased voltage but if the pump power is larger than ~ 12 mW, THz pulses can be at their saturation points and their power values can be stay in constant [19].

Secondly, we analyze the results obtained from the theoretical calculation method called “Open-Circuit Voltage”. By using this method we get average THz power in the range of nW - μW as shown in the Table [4.1] that are more meaningful results according to the ones obtained from the same experimental systems.

REFERENCES

[1] Y. C. Shen, P. C. Upadhya, E. H. Linfield, et al., *Terahertz generation from coherent optical phonons in a biased GaAs photoconductive emitter*, Appl. Phys. Lett., vol. 83, (2003) 15

[2] O. Ridge, *Blinded By The Light At 20,000 THz*, Tech. Space, 2003

[3] Z. Wang, Student member, *Generation of terahertz radiation via nonlinear optical methods*, IEEE Trans. On Geosci. And Remot. Sens. vol. 1, no. 1, 2100

[4] Jason D. Readle, *Terahertz time-domain spectroscopy*, http://online.physics.uiuc.edu/courses/phys498os/fall07/Reports%5CReadleJD%20-%20THz-TDS.pdf

[5] D. Auston and K. Cheung, *Coherent time-domain far-infrared spectroscopy*, J. Opt. Soc. Am. B, vol. 2, pp. 606-612, 1985

[6] The IEEE Boston Section Techsite, *http://www.ieeeboston.org/edu05s/2005fall/terahertz_systems.htm*, 28 June 2007

[7] S. Wang, B. Ferguson, D. Abbott, et al., *T-ray Imaging and Tomography*, J. Bio. Phys., vol. 29, pp. 247-256, 2003

[8] P. H. Siegel, *Terahertz Technology*, IEEE Trans. Mic. Theo. Tech. vol. 50, no. 3, 2002

[9] D. M. Mittleman, R. H Jacobsen, R. Neelamani, et al., *Gas sensing using terahertz time domain spectroscopy*, Appl. Phys. B., vol. 67, pp. 379-390, 1998

[10] D. Dragoman and M. Dragoman, *Terahertz fields and applications*, Prog. In Quant. Elec., vol. 28, pp. 1-66, 2004

[11] M. Tani, M. Herrmann and K. Sakai, *Generation and detection of terahertz pulsed radiation with photoconductive antennas and its application to imaging*, Meas. Sci. Technol., vol. 13, pp. 1739-1745, 2002

[12] C. Rullière, *Femtosecond Laser Pulses: Principles and Experiments (2nd Ed.),* New York: Springer, ISBN 0-387-01769-0, 2004.

[13] G. D. Reid, K. Wynne, *Ultrafast Laser Technology and Spectroscopy*, pp. 13644-13670, 2000

[14] BBC Home, Everything / Maths. Science & Technology/ Engineering, *http://www.bbc.co.uk/dna/h2g2/A897609*, 10 March 2003

[15] K. Wynne, J. J. Carey, *An integrated description of terahertz generation through optical rectification, charge transfer, and current surge*, Optic. Commun. vol. 256, pp. 400-413, 2005

[16] G. Zhao, R. N. Schouten, N. van der Valk, et al., *Design and performance of a THz emission and detection setup based on a semi-insulating GaAs emitter*, vol. 73, no. 4, Rev. Sci. Instrum., 2002

[17] S. G. Park, M. R. Melloch and A. M. Weiner, *Comparison of terahertz waveforms measured by electro-optic and photoconductive sampling*, Appl. Phys. Lett., vol. 73, no. 22, 1998

[18] Q. Chang, D. Yang, L. Wang, *Broadband THz generation from photoconductive antenna*, Prog. In Elec.mag. Researc. Symp., 2005

[19] J. Zhang, Y. Hong. S. L. Braunstein, et al., *Terahertz pulse generation and detection with LT-GaAs photoconductive antenna*, IEE Proc. –Optoelectron., vol. 151, no. 2, 2004

[20] C. A. Schmuttenmaer, *Exploring dynamics in the far-infrared with terahertz spectroscopy*, Chem. Rev. vol. 104, pp. 1759-1779, 2004

[21] S. Wei, H. Lei, *Theoretical study of field intensity of THz radiation from GaAs large-aperture photoconductive antennas*, Chin. Phys. Lett. vol. 23, no. 10, 2006

[22] D. H. Auston, M. C. Nuss, *IEEE member, Electrooptic generation and detection of femtosecond electrical transients*, IEEE J. of Quant. Elec., vol. 24, no. 2, 1988

[23] Z. Zhen-Yu, H. Sophie, T. Jérôme, *THz generation by optical rectification and competition with other nonlinear processes*, vol. 25, no. 5, 2008

[24] A. Bonvalet, M. Joffre, J. L. Martin, et al., *Generation of ultrabroadband femtosecond pulses in the mid-infrared by optical rectification of 15 fs light pulses at 100 MHz repetition rate*, vol. 67, no. 20, 1995

[25] Y.Cai, I. Brener, J. Lopata, et al., *Coherent terahertz radiation detection: Direct comparison between free-space electro-optic sampling and antenna detection*, Appl. Phys. Lett. vol. 73, no. 4, 1998

[26] Q. Chen, M. Tani, Z. Jiang, et al., *Electro-optic transceivers for terahertz-wave applications*, J. Opt. Soc. Am. B, vol. 18, no. 6, pp. 823-831, 2001

[27] S. Casalbuoni, H. Schlarb, B. Schmidt, et al., *Numerical studies on the electro-optic detection of femtosecond electron bunches*, Phys. Rev. ST Accel. Beams, vol. 11, no. 072802, 2008

[28] N. C. J. van der Valk, T. Wenckebach, P. C. M. Planken, *Full mathematical description of electro-optic detection in optically isotropic crystals*, J. Opt. Soc. Am. B, vol. 21, no. 3, 2004

[29] P. C. M. Planken, H. J. Bakker, T. Wenckebach, et al., *Measurement and calculation of the orientation dependence of terahertz pulse detection in ZnTe,* J. Opt. Soc. Am. B, vol. 18, no. 3, 2001

[30] Model SR830 DSP Lock-In Amplifier, *http://www.thinksrs.com/downloads/PDFs/Manuals/SR830m.pdf*

[31] Optics & Laser Europe, *SR830 Lock-In Amplifier*, http://iopp.fileburst.com/old/old_02_139.pdf, Issue 139, May 2006

[32] M. Tani, S. Matsuura, K. Sakai, et al., *Emission characteristics of photoconductive antennas based on low-temperature-grown GaAs and semi-insulating GaAs*, Appl. Opt. vol. 36, no. 30, 1997

[33] Batop Optoelectronics, *PCA - Photoconductive Antenna for THz Applications*, http://www.batop.de/informations/PCA_infos.html,

[34] M. Born and E. Wolf, *Principles of Optics*, 7th (expanded) edition

[35] S. Mickan, D. Abbott, J. Munch, et al., *Analysis of system trade-offs for terahertz imaging*, vol. 31, pp-503–514, 2000

[36] D. Baird, R. I. G. Hughes, H. Hertz, et al., *Heinrich Hertz: Classical Physicist, Modern Philosopher*, New York: Springer, ISBN 079234653X, 1998

[37] W. James, *Antenna Here Is a Dipole*, http://www.arrl.org/tis/info/pdf/9106023.pdf

[38] V. K. Salvia, *Antenna and Wave Propagation*, http://books.google.co.uk/books?id=MiL42MSE3KEC&printsec=frontcover&dq=antenna+and+wave+propagat%C4%B1on&hl=tr

[39] P. C. Upadhya, W. Fan, A. Burnett, et al., *Excitation-density-dependent generation of broadband terahertz radiation in an asymmetrically excited photoconductive antenna*, Opt. Lett. Vol. 32, no.16, 2007

[40] K. Sakai (Ed), *Terahertz Optoelectronics*, New York: Springer, 2005

[41] J. S. Hwang, H. C. Lin, K. I. Lin, et al., *Terahertz radiation from InAlAs and GaAs surface intrinsic-N+ structures and the critical electric fields of* semiconductors, Appl. Phys. Lett., vol. 87, no. 121107, 2005

[42] Lecture notes, *Notes for Antennas I*, www.engr.pitt.edu/ELECTRICAL/faculty-staff/falk/ee1266/Fall%202006/.../EE1266_Antenna_1%20modified%20by%20jf.doc.

[43] S. G. Park, M. R. Melloch, A. M. Weiner, et al., *Analysis of Terahertz waveforms measured by photoconductive and electrooptic sampling*, vol. 35, no. 5, 1999

[44] G. A. Balanis, *Antenna Theory*, New York: Wiley, 1982

[45] Chapter 2 Historical Landscape, *http://digital.library.adelaide.edu.au/dspace/bitstream/2440/37962/9/03chapter2.pdf*, pp. 13-28

[46] M. van Exter, D. R. Grischkowsky, *Characterization of an optoelectronic terahertz beam system*, IEEE Trans. on Mic. The. And Tech., vol. 38, no. 11, 1990

[47] G. Fraser, *The New Physics for the twenty-first century (2nd Ed.)*, Cambridge University Press, ISBN 0521816009, 2006

[48] E. C. Jordan, K. G. Balmain, *Electromagnetic Waves and Radiating Systems (2nd Ed.),* Prentice-Hall Inc., 1968

[49] M. M. Weiner, *Monopole Antennas*, CRC Press, ISBN 0824704967, 2003

[50] C. R. Paul, *Introduction to Electromagnetic Compatibility*, Wiley-Interscience, 1992